Hierarchical Lineage Tracing Reveals Diverse Pathways of AML Treatment Resistance

Rachel Saxe[1,2], Hannah Stuart[1,3], Abigail Marshall[1,2], Fahiima Abdullahi[5], Zoë Chen[4], Francesco Emiliani[1,2], Aaron McKenna[1,4]

[1]Molecular and Systems Biology, Dartmouth College, Hanover, NH
[2]Molecular and Cellular Biology Program, Dartmouth College, Hanover, NH
[3]Quantitative Biomedical Science Program, Dartmouth College, Lebanon, NH
[4]Dartmouth Cancer Center, Dartmouth College, Lebanon, NH
[5]The Dartmouth MD-PhD Undergraduate Summer Fellowship Program, Lebanon, NH

Abstract

Cancer cells adapt to treatment, leading to the emergence of clones that are more aggressive and resistant to anti-cancer therapies. We have a limited understanding of the development of treatment resistance as we lack technologies to map the evolution of cancer under the selective pressure of treatment. To address this, we developed a hierarchical, dynamic lineage tracing method called FLARE (Following Lineage Adaptation and Resistance Evolution). We use this technique to track the progression of acute myeloid leukemia (AML) cell lines through exposure to Cytarabine (AraC), a front-line treatment in AML, in vitro and in vivo. We map distinct cellular lineages in murine and human AML cell lines predisposed to AraC persistence and/or resistance via the upregulation of cell adhesion and motility pathways. Additionally, we highlight the heritable expression of immunoproteasome 11S regulatory cap subunits as a potential mechanism aiding AML cell survival, proliferation, and immune escape in vivo. Finally, we validate the clinical relevance of these signatures in the TARGET-AML cohort, with a bisected response in blood and bone marrow. Our findings reveal a broad spectrum of resistance signatures attributed to significant cell transcriptional changes. To our knowledge, this is the first application of dynamic lineage tracing to unravel treatment response and resistance in cancer, and we expect FLARE to be a valuable tool in dissecting the evolution of resistance in a wide range of tumor types.

Introduction

Acute myeloid leukemia (AML) is a heterogeneous hematological malignancy that has served as a model of clonal evolution in response to treatment[1–4]. AML subtypes and risk categories have long been primarily defined by cytogenetics, mutation status, and structural genomic variations. However, with recent advances in RNA sequencing, transcriptome profiling has begun to uncover further leukemic disease states, dependencies, and prognostic signatures[5–7]. Upon diagnosis, most patients are treated with induction therapy, including an aggressive cycle of Cytarabine (AraC). While ~80% of patients reach remission following induction, most will relapse[8]. Single-cell RNA sequencing (scRNA-seq) of matched pre- and post-treatment patient bone marrow samples show patients have dramatic disease landscape changes following AraC treatment[2].

It remains unclear how resistance to AraC evolves in many AML patients. Are AraC-resistant subclones pre-existing, or does resistance emerge de novo in rare subpopulations? Does the resistant phenotype pass through multiple intermediate states or emerge in a punctuated evolution? Previous studies have investigated the origin of chemoresistant cell populations in various cancer types[9–12]. Shaffer et al. concluded that while rare subpopulations of cells exhibit pre-resistant-like phenotypes, melanoma cells could transiently shift to a resistant phenotype upon treatment in vitro[11]. In contrast, Yan et al. identified a subpopulation of TP53-mutated AML cells in treatment-naïve samples believed to be the source of future AraC-resistant populations[9]. These studies highlight that treatment failure and resistance are likely driven by diverse disease, drug, and likely, patient-specific mechanisms. While individual patients may display unique lineage developments and gene expression profiles, pathway alterations that arise frequently can be exploited for treatment response prediction, patient stratification, and development of targeted therapies.

We set out to develop a cellular lineage tracing system to record the evolutionary steps of AraC treatment resistance in AML. Here, we present FLARE (Following Lineage Adaptation and Resistance Evolution), a multi-tiered lineage tracing approach, which we use to identify clonal patterns of drug response and expansion in vitro and in vivo. Using advances in CRISPR lineage tracing, we track the evolution of cell fate independently of cell state, recording the relationship between cells in small, integrated recorders, which can be used to recover cellular ‘phylogenetic’ trees[13,14]. This lineage information alone can uncover treatment response

patterns, but when paired with transcriptomic data, it acts as a window into disease evolution. CRISPR lineage recording has been previously used to characterize clonal evolution through tumorigenesis and metastasis, yet the effect of treatment has yet to be explored[14,15].

We use FLARE to uncover multiple heritable and lineage-specific gene modules associated with drug response with matched outcomes in pediatric AML patient survival. FLARE lineage patterns uncovered a highly heritable gene signature in treatment-naive AML cells involved in cell-adhesion-mediated drug resistance (CAM-DR) pathways, the expression of which leads to lineage branch survival and expansion under AraC exposure. In addition, we identified an AML lineage-dependent upregulation of immunoproteasome subunits, with further upregulation leading to improved expansion in vivo. Finally, we validated the clinical relevance of our findings using RNA sequencing data from the pediatric TARGET AML cohort and discover bone marrow and peripheral blood-specific expression profiles significantly associated with patient outcomes.

Results

Hierarchical lineage recording in AML

We set out to develop a dynamic cellular lineage tracing system to model the fitness landscape of AML in vitro and in vivo. Expanding on our previous macsGESTALT lineage tracing system[14], we created a hierarchical system, capturing lineage information at three levels (**Figure 1A-B**). At the top level, FLARE encodes founder populations using a unique combination of static tags accompanying the lineage recorders when integrated into the genome. Within each labeled founder population, individual clones are divided into sub-populations with a second round of tags integrated with the Cas9 cassette. This Cas9 integration also begins the dynamic lineage recording, creating insertions and deletions (indels) within the lineage recorders, capturing sub-clonal lineage information. We can then use computational methods to generate a phylogenetic tree of cell relationships within these founder and clonal populations from these indels. This three-level structure (founder, clone, and subclonal lineage information) allows FLARE to track dynamics across time and to compare sister populations in both the control and treatment arms, in vitro and in vivo.

We first engineered this approach in the C1498 cell line, a syngeneic mouse model of AML compatible with transplantation into immune-competent C57BL/6 mice. Despite being long-passaged, C1498 cells are known to be heterogeneous, making them an optimal model for investigating the diversity of clonal treatment response[16]. We established 11 founder populations from individually isolated cells through successive engineering rounds (**Figure S1A-B)**. Sequencing revealed a unique set of founder tags for each population, varying from 19 to 30 integrations (**Figure S1C**). These isolated founders are heterogeneous, with a wide range of growth kinetics (**Figure S1D**). We found no putative driver mutation differences between individual founders using whole-genome sequencing that would explain this heterogeneity.

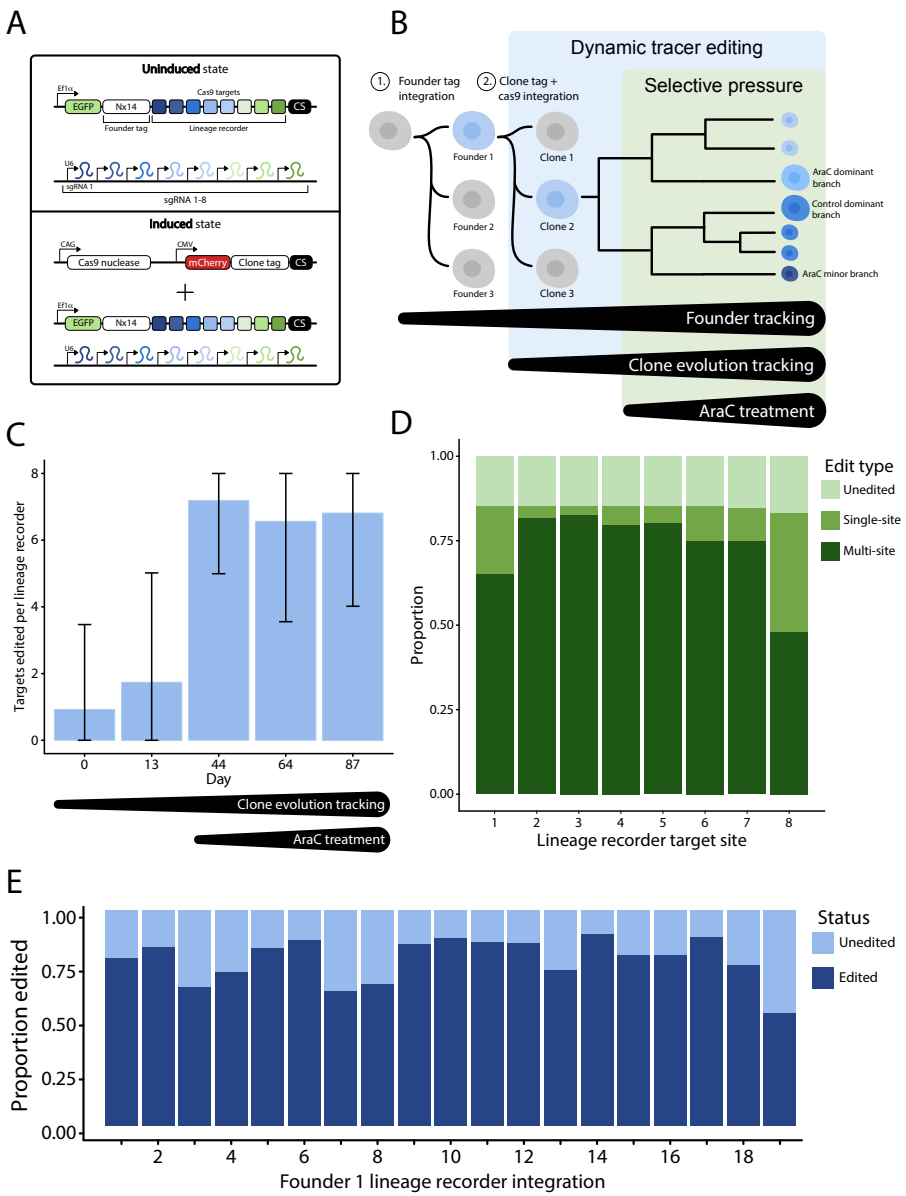

<u>Figure 1</u>: FLARE lineage tracing system allows for hierarchical tracking of cell populations through time. (**A**) Constructs required for FLARE lineage tracing. The top panel includes FLARE-miniV10-10X-UMI (founder tag + lineage recorder) and FLARE-pbV10g-neo (Cas9 guide sequences). We then electroporate the FLARE-pbCas9-tag-mCherry into cells (bottom panel), tagging each clone and activating CRISPR lineage recording. (**B**) The resulting cells record lineage information at 3 levels, (1) founder, (2) clonal, and (3) subclonal (CRISPR recordings). AraC treatment selective pressure is introduced following the initiation of lineage recorder editing. (**C**) Lineage recorders are readily edited following the introduction of Cas9. Editing rates plateau after around 44 days of Cas9 exposure. (**D**) Following 87 days of Cas9 exposure lineage recorder edits are primarily composed of multi-site editing events, with a smaller proportion of edits impacting single sites. Around 15% of lineage recorder sites remain unedited through 87 days of editing. (**E**) Editing rates are consistent across lineage recorder integrations within the C1498-FLARE Founder 1 population.

Characterizing lineage recording

Next, we set out to test the lineage recording capacity of our engineered cells. We activated CRISPR recording by integrating the Cas9 construct into the genome (**Figure 1A-B**). After electroporation and sorting, we sampled Cas9-positive C1498-FLARE cell populations at days 13, 44, 64, and 87 and sequenced the lineage recorders to characterize Cas9 editing (**Figure 1C**). Recording proportions suggest the bulk of lineage recorder editing occurs between day 13 (22.61% of recorders contain >= 1 edit) and 44 (99.97% >= 1 edit). Editing rates remained high through at least day 87 (85.93% >= 1 edit), with continuing fluctuations in editing patterns due to population drift. Editing patterns were comparable between lineage recorder target sites (**Figure 1D)**, and most edits span multiple target sites with a smaller proportion of edits affecting individual targets. Approximately 15% of sequenced lineage recorder targets remained unedited, indicating our ability to trace lineage over at least 87 days without saturation.

We further characterized the response of individual recorder integrations with a single founder group, founder 1 (F1), containing 19 unique integrations. All integrations were active recorders displaying diverse editing outcomes (**Figure 1E**). For all founder populations assessed, individual recording events tended to be large, spanning 3.075 targets on average, and each recorder contained an average of 2.57 individual recording events. While edits consisting of large deletions can lead to loss of lineage information, we could still reliably reconstruct lineage trees with an average depth of 5.566 nodes over relevant timescales. We attribute this to this system's high lineage recording capacity, with engineered cells containing between 152 and 240 CRISPR target sites per cell.

Clonal treatment response and tree generation in vitro and in vivo

Confident in our ability to record and recover cellular lineage information, we set out to characterize C1498-FLARE population dynamics in response to the chemotherapy AraC in vitro and in vivo (**Figure 2A)**. To recreate the heterogeneity observed in leukemia patients, we pooled four C1498 founder groups for our starting population, which was then used for both in vitro and in vivo AraC treatment.

By day 43 of in vitro AraC treatment we observed two distinct growth phenotypes. Our AraC-resistant flask displayed rapid growth and a 10-fold higher ED50 than control cell populations (**Figure S2A**). We also observed a separate flask phenotype, where cells appeared to be "persistent", displaying minimal proliferation and cell numbers too low for ED50 determination. We sequenced 27,237 single cells from the untreated, resistant, and persistent flasks. Treated cells clustered into distinct groups predominantly separated by flask phenotype (**Figure 2B**). We successfully captured founder tags and lineage recorders from 100% of single cells and clone tags from 31.9%. After filtering, quality control, and lineage assignment, 25,489 single cells were

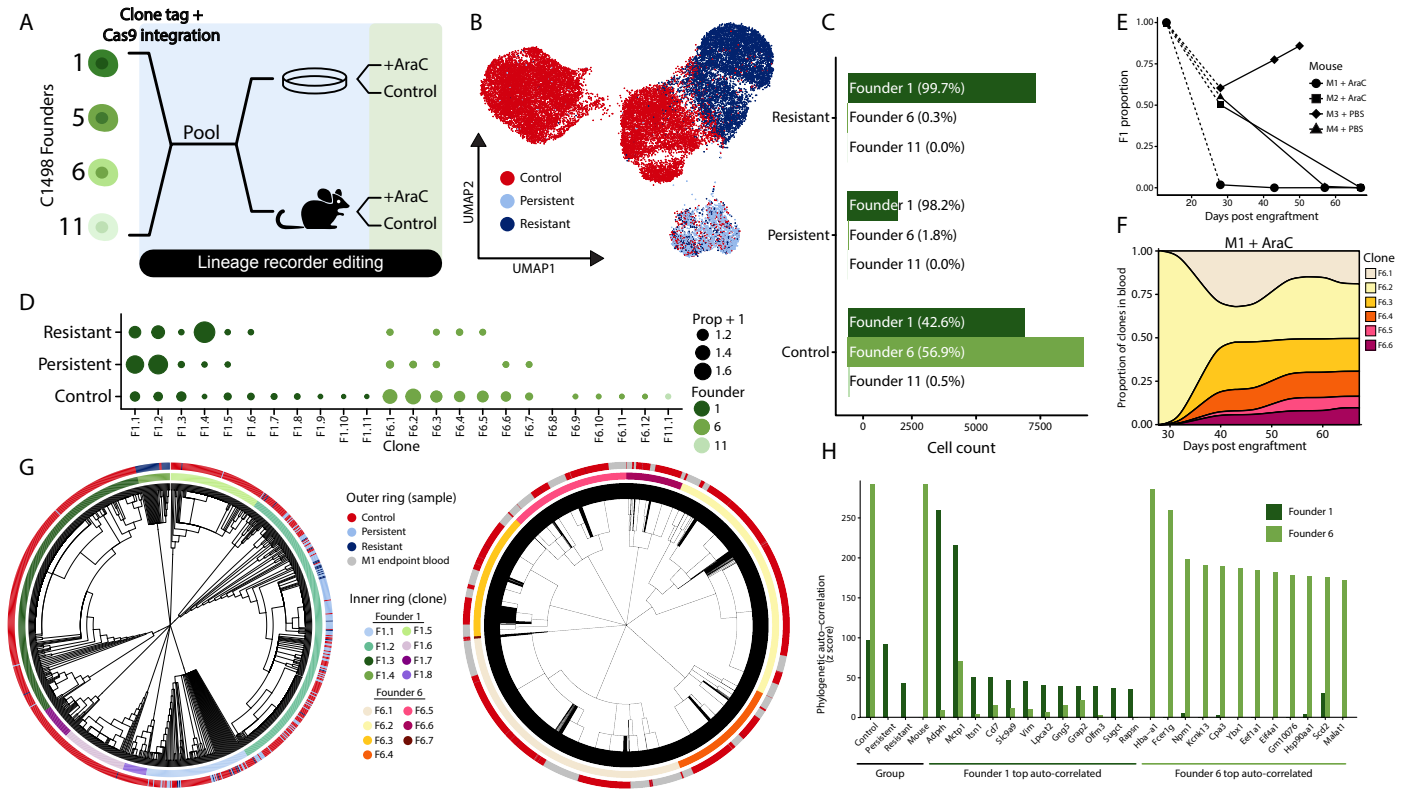

Figure 2: FLARE lineage tracing tracks founder and clone-level evolution in response to AraC treatment in vitro and in vivo. (**A**) Experimental design of lineage tracing C1498-FLARE AML cells in vitro and in vivo. (**B**) Single-cell sequencing of C1498-FLARE cells following 43 days of in vitro AraC treatment. Cells cluster into distinct groups associated with their sample (red - no AraC; dark blue - AraC resistant flask; light blue - AraC persistent flask). (**C**) Founder proportions in each sample display increased survival of F1 cells under AraC treatment in both the resistant and persistent populations. (**D**) Clone populations detected within each sample, ordered by founder and clone size. (**E**) Founder and clone tags detected in blood draws from mice engrafted with C1498-FLARE cells were used to calculate the proportion of circulating leukemic cells belonging to F1 compared to F6. Day 13 proportions were computed using founder tag sequencing and are connected to day 28 with dashed lines. All other timepoint proportions were calculated using clone tag sequencing, normalized for differences in the number of integrations. The F1 proportion was defined as the F1 average tag count divided by the sum of F1 and F6 average tag counts. Untreated mouse M3 was euthanized on day 50 due to disease progression. The remaining mice were euthanized on day 67. (**F**) Bulk sequencing of clone tags detected in blood draws from mouse M1 following AraC treatment on day 13. Clone tag reads were used to determine the clonal proportions of leukemic burden in the blood from day 28 to day 67. (**G**) Phylogenetic reconstruction of founders F1 (left) and F6 (right) generated from single-cell sequencing of in vitro C1498-FLARE lineage tracing and single-cell sequencing of endpoint blood and bone marrow from treated mouse M1. (**H**) Heritability of both sample features and genes for founder 1 and founder 6 computed with PATH.

161 assigned to founder groups, of which 5,468 were successfully assigned to clones. Founder tag
162 sequencing revealed in vitro fitness differences: in untreated flasks, founder 1 (F1) and founder
163 6 (F6) dominated (43% and 57% of cells, respectively), and few founder 11 (F11) cells were
164 detected (<0.5% of cells). F1 and F6 control cells clustered separately, suggesting distinct
165 founder-specific transcriptomes (**Figure S2B)**. In contrast, treated populations were primarily
166 composed of F1 with few F6 (<0.7%) and zero F11 cells. F5 was outcompeted in all conditions
167 (**Figure 2C)**.
168
169 We performed differential gene expression analysis between founder groups, focusing on F1
170 and F6 in the control setting. F1 lineages were characterized by high expression of Nkain3,
171 Wnt6, and Chl1 (**Table S1**). In contrast, F6 lineages were characterized by high expression of
172 Sox2ot, Tnni1, and Tnnt1 (**Table S2**). GSEA results indicated enrichment of multiple Hallmark
173 pathways in F6 compared to F1, including MYC targets V1, oxidative phosphorylation, and
174 MTORC1 signaling (**Figure S2C**). Enriching these oncogenic pathways likely contributed to the
175 success of F6 in the absence of treatment. Since these pathways have well-established roles in
176 chemoresistance, we expected F6 to display a survival advantage under AraC treatment[17–20].
177 Unexpectedly, F6 was almost fully out-competed by F1 in the presence of AraC (**Figure 2C)**.
178
179 We then explored founder F1's competitive advantage over F6 and the other founders during
180 treatment. Within F1 populations, there was a distinct and divergent selection of specific clones
181 in AraC-treated and control flasks (**Figure 2D**). The highest proportion of persistent cells
182 belonged to clones F1.1 and F1.2, while the highest proportion of resistant cells belonged to
183 F1.4. F1 cells have a clear survival advantage through in vitro AraC treatment, but the
184 outgrowth of different clones in treated replicates suggests clone-specific responses that
185 contribute to population growth dynamics.
186
187 To identify F1 clone-specific treatment responses, we analyzed differentially expressed genes
188 between control, resistant, and persistent-dominant clones (**Table S3**). Our dominant clone in
189 the resistant population, F1.4 (**Figure 2D**), expressed high levels of IgII1 and Evac1 compared
190 to other resistant cells. Clones F1.1 and F1.2 were successful in both persistent and resistant
191 populations; when we compared their control gene expression to all other F1 clones, a
192 transcriptional signature containing Grap2, Trat1, and Ldlrad4 emerged (**Figure S2D**). Trat1 is
193 involved in the regulation of T cell receptors and expression is associated with immune cell
194 infiltration and improved survival in breast, ovarian, and lung cancer [21–23], Ldlrad4 is a negative

195 regulator of TGF-beta signaling [24,25], and expression promotes the proliferation and migration of
196 hepatic cancer cells and is downregulated in CD34+ cells from patients with MDS [26]. Consistent
197 with the upregulation of Ldlrad4 expression in F1.1 and F1.2 control cells, sister cells of both
198 clones in the persistent population display high Ldlrad4. We also identified clones with pre-
199 existing lineage-specific expression patterns. Cells belonging to clone F1.3 tended to colocalize
200 and shared high expression of Adprh and Mctp1 (**Figure S2E-F)**. These genes highlighted by
201 differential gene expression analysis do not have well-established roles in AML.
202
203 In parallel to our in vitro treatment assay, we injected immune-competent C57BL/6 KH2[27] mice
204 with 25k of the pooled founder starting population to induce leukemia with lineage tracing
205 capacity (**Figure 2A)**. Mice were then treated with AraC to a dose comparable to that given to
206 patients in one round of 7+3 induction chemotherapy[9]. We used bulk lineage sequencing to
207 estimate founder and clone dynamics from blood draws of circulating leukemia cells. Contrary to
208 our in vitro results, F6 outcompeted other founder populations in vivo in all but one mouse
209 (**Figure 2E**). This bottlenecking occurred sometime between day 28, when all founders were
210 detectable in control and treated mice (**Figure S3A),** and euthanasia on day 67. A selective
211 sweep was nearly complete in treated mouse M1 (>99.9% F6 by day 43), treated mouse M2
212 (100% F6 by day 67), and untreated mouse M4 (>99.9% F6 by day 57). Control mouse M3's
213 leukemic burden was composed of >77.5% F1 by day 43, and this increased to >85.9% on day
214 50 when M3 was euthanized due to symptomatic disease.
215
216 We then focused on the within-founder clone tag sequences seen in blood draws. Interestingly,
217 M1 displayed sustained clonal diversity split amongst F6.1, F6.2, F6.3, F6.4, and F6.5,
218 indicating these clones survived AraC treatment and had comparable fitness during post-
219 treatment outgrowth. In contrast, blood samples from M3 were primarily dominated by F1's
220 clone F1.2 by day 43 (**Figure S3C)**. Blood samples from M2 and M4 did not contain enough
221 overlap with our known clone tags to infer population dynamics, likely representing diversity not
222 captured in our single-cell sequencing at end-point.
223
224 To further examine the lineage identities and transcriptomes of cells surviving in vivo treatment,
225 we sequenced 10,473 and 6,344 cells from blood and bone marrow, respectively, of treated
226 mouse M1 displaying sustained F6 clonal diversity. Non-leukemic cells clustered by cell type,
227 and leukemic cells were identified by founder and clone tags (**Figure S3D-E)**. Of the leukemic
228 cells, 6 and 6,053 belonged to founders F1 and F6, respectively. Clone groups were assigned to

229 2,002 single cells, 702 belonging to clone F6.1. The remaining clone assignments were split
230 between F6.2, F6.3, F6.4, and F6.5 (**Figures 2F, S3B**). We also detected low frequencies of
231 cells belonging to F6.6 and F6.8. These single-cell sequencing results matched the population
232 detected in bulk sequencing, confirming our ability to reconstruct founder and clone patterns
233 from limited samples, such as blood draws, using FLARE lineage tracing.
234
235 We then created phylogenetic trees for F1 and F6 using FLARE lineage recorder indels
236 captured with our in vitro and in vivo scRNA-seq (**Figure 2G)**. To identify heritable gene
237 expression patterns associated with the development of AraC resistance, we conducted lineage
238 autocorrelation analysis on founder trees using PATH (**Figure 2H**)[28]. PATH highlighted genes
239 previously identified by differential gene expression analysis as highly cross-correlated with
240 resistant and/or persistent cell identities in the F1 tree (**Figure S3F**). These genes include
241 Olfm3, a gene associated with anoikis resistance in AML cells[29], and Cd7, the expression of
242 which in AML is a prognostic risk factor[30–32]; both genes were significantly upregulated in AraC
243 persistent cells. Genes such as Adprh and Mctp1, associated with the F1.3 clone branch, were
244 also strongly heritable but expressed primarily in a subset of control cells.
245
246 These initial experiments with C1498-FLARE cells allowed us to optimize the lineage tracing
247 system and test our ability to track leukemic lineage in immune-competent mice. With FLARE,
248 we successfully identified highly heritable genes selected for through AraC treatment that
249 contribute to drug persistence and resistance.

250 Clonal treatment response and tree generation in human AML cells

251 We next engineered FLARE lineage recording human HL60 cells, a model of FAB-M2 AML[33].
252 We seeded 500 HL60-FLARE founder cells, expanded, and split into parallel cultures (**Figure**
253 **3A**). This starting pool expands on the transcriptional landscape sampled in C1498-FLARE cells
254 while maintaining sister founder populations in the control and treatment arms. Similarly to
255 C1498-FLARE cells, our resulting HL60-FLARE cells clustered in distinct groups based on AraC
256 treatment in vitro (**Figure 3B**). However, unlike C1498-FLARE cells, AraC-treated HL60-FLARE
257 cells in different flasks clustered together despite different regrowth rates (**Figure S4A**). AraC-
258 treated flask A reached cell concentrations comparable to untreated HL60-FLARE cells by day
259 80 of AraC treatment, so we posited these cells would align transcriptionally with C1498-FLARE
260 resistant cells. Surprisingly, differential expression analysis uncovered the upregulation of genes
261 shared with AraC-persistent C1498 F1 cells such as VIM, PSD3, CRIP1, and S100A4 (**Table**

S4). AraC-treated flask B displayed slower growth dynamics but shared flask A's transcriptional profile (**Table S5**).

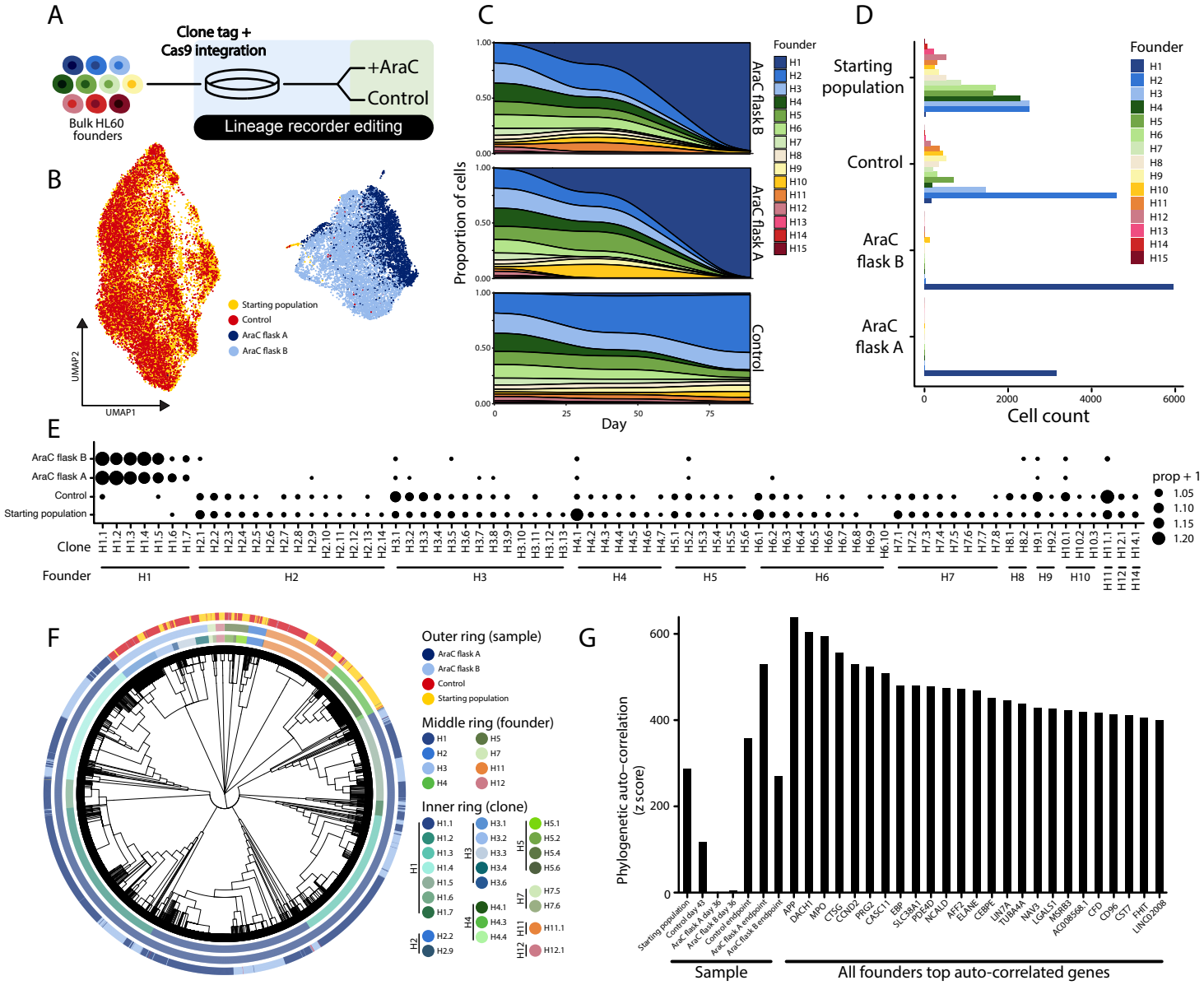

Figure 3: Founder and clone-level selection of founder H1 in response to AraC treatment in human HL60 AML cells. (**A**) Experimental design of HL60-FLARE AML lineage tracing in vitro. (**B**) Single cell sequencing of HL60-FLARE cells following 89 days of in vitro AraC treatment. Cells cluster into distinct groups associated with their sample (yellow - starting population; red - no AraC; dark blue - AraC flask A; light blue - AraC flask B). (**C**) Clone population fluctuations for each flask throughout the experiment. (**D**) Founder proportions in each sample display increased survival of founder H1 cells under AraC treatment in both flask A and B. (**E**) Clone populations for each sample at experimental endpoint, ordered by founder and clone size. (**F**) Phylogenetic reconstruction of HL60-FLARE cells generated from single cell sequencing of in vitro lineage tracing. (**G**) Heritability of both sample features and genes for all HL60-FLARE founders computed via PATH.

Single-cell sequencing of founder and clone tags was used to cluster cells into 15 founder populations (H1-H15), individually composed of 1-14 clones. Sequencing from cells collected at the experiment start, midpoint, and endpoint were used to determine founder proportions over time for each flask. All 15 HL60 founders were detected in the experimental starting population and the control flask at endpoint (**Figure 3C-D**). There was an extensive bottleneck in all cultured populations, regardless of treatment. Untreated endpoint cells were most likely to descend from H2, while both AraC-treated flasks consisted primarily of cells belonging to H1. Both treated flasks maintained diversity within H1 on the clonal level, with most cells being evenly split between clones H1.1, H1.2, H1.3, H1.4, and H1.5 (**Figure 3E**).

The success of H1 in both treated flasks suggests a founder-specific propensity for treatment resistance prior to treatment onset. This is also supported by the comparable fitness of H1 clonal populations, indicating the lack of clone-specific resistance evolution. We used differential gene expression analysis to explore H1-specific expression patterns in the presence and absence of treatment to determine whether H1 cells were consistently differentiated from other founders or were primed for reprogramming following the introduction of AraC. Pre-experiment and endpoint control H1 cells shared the upregulation of 104 genes (**Table S6**). Many of these genes were also upregulated in AraC-resistant H1 cells compared to other founders, including MKX, APBA2, LAMP5, CAMK2D, and NAV3.

We turned to phylogenetic reconstruction and heritability analysis to further dissect the H1's resistance mechanisms. We used lineage recorder indel patterns to reconstruct phylogenetic trees for each clone population. These clonal trees were merged to create founder-level lineage trees, and founder-level trees were merged to create the HL60 population tree (**Figure 3F**). PATH analysis on the population tree revealed many highly heritable genes associated with evolution with and without AraC, including genes previously implicated in AML prognosis and treatment response, such as MPO (**Figure 3G**). This analysis also indicated significant heritability of genes previously identified as upregulated in treatment-naive H1 cells.

Identification of pro-leukemic transcriptional programs associated with pre-AraC-resistant lineages

To better understand broad transcriptomic changes over AraC-induced clonal evolution, we generated lineage-dependent gene modules for C1498-FLARE F1 and F6 trees, and the HL60-

297 FLARE population tree using Hotspot (**Figure 4A-B, Table S3, Table S7**)[34]. Jaccard indices
298 revealed significant similarity between a number of HL60 and C1498 modules, indicating shared
299 mechanisms across our two experimental lines (**Figure 4C, S4B-C**). Moreover, expression of
300 these modules within the lineage structure showed founder and clone-specific enrichment
301 (**Figure 4D**).
302

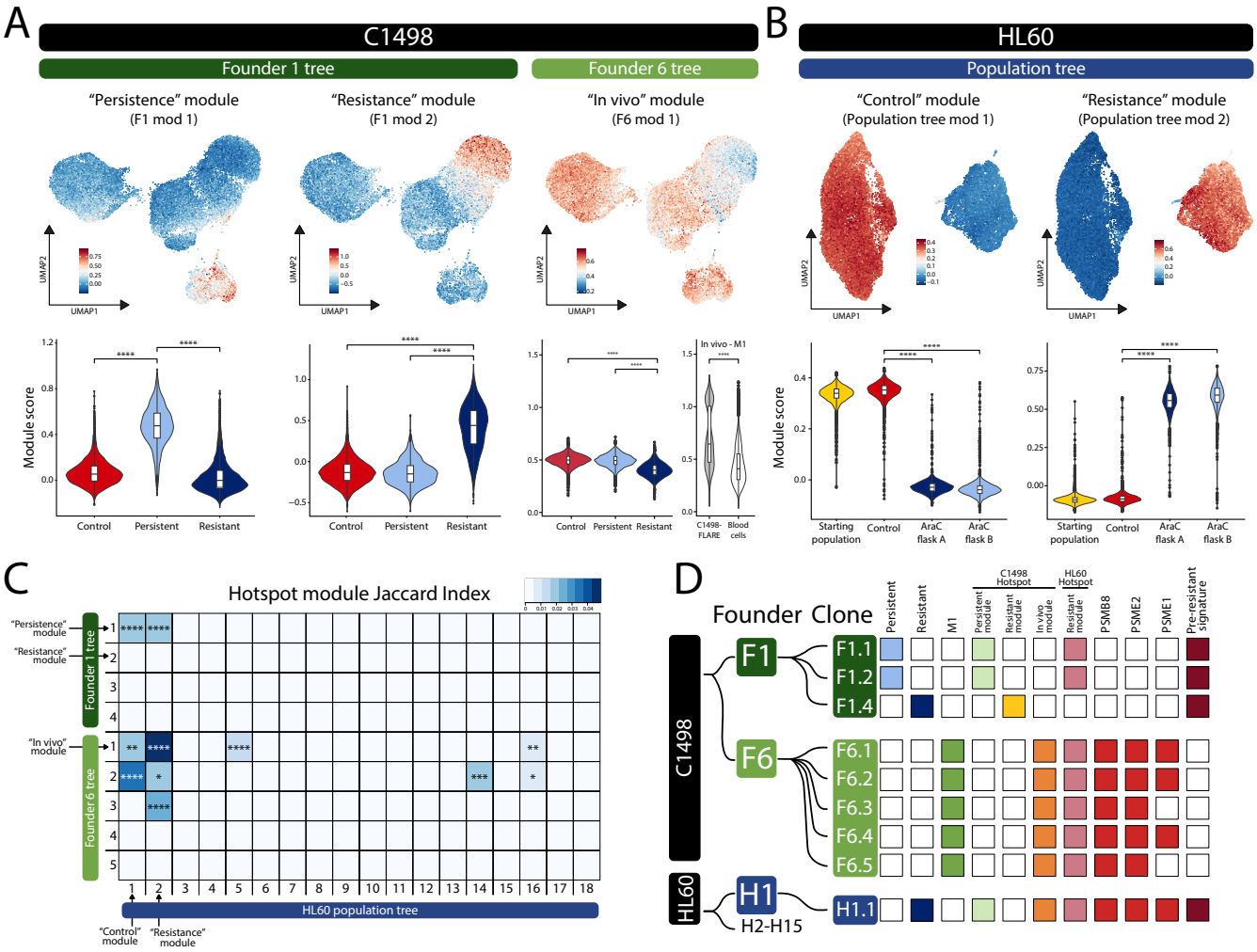

<u>Figure 4</u>: Hotspot gene modules reveal heritable AraC response mechanisms common to mouse and human AML cells. (**A**) Feature and violin plots for selected C1498-FLARE Hotspot modules. Significance determined by wilcoxon rank sum test with Bonferroni correction. (**B**) Feature and violin plots for selected HL60-FLARE Hotspot modules. Significance determined by wilcoxon rank sum test with Bonferroni correction. (**C**) Jaccard Index similarity comparing C1498-FLARE and HL60-FLARE Hotspot modules. Square color indicates Jaccard Index, asterisks represent BH-corrected P-value significance levels. (**D**) Schematic showing the lineage relationships of C1498-FLARE and HL60-FLARE clones. The first three columns to the right of the clone labels indicate the setting in which each clone had a survival advantage, either in the Ara-C persistent population (a growth phenotype we only saw in C1498-FLARE populations), resistant population, or in AraC-treated mouse M1's peripheral blood and bone marrow. The next four columns to the right indicate modules upregulated in each clone. The next three columns indicate whether immunoproteasome gene PSMB8 and 11S regulatory cap genes PSME1 and PSME2 were significantly upregulated in the AraC treated populations. The rightmost column indicates the upregulated expression of the pre-resistant signature in AraC-treated populations.

303 We first focused on the overlap between HL60-FLARE “resistance” module 2 and C1498-
304 FLARE “persistence” F1 module 1 (**Table S9**), the most heritable modules enriched in treatment
305 conditions. The HL60-FLARE “resistance” module was distinctly enriched in all AraC-treated
306 cells (**Figure 4B**), while the C1498-FLARE “persistence” module was associated with AraC-
307 persistent populations (**Figure 4A**). The HL60 resistance module was primarily expressed in the
308 H1 founder population and contained many genes found to be distinctly upregulated in
309 treatment-naive H1 cells (**Table S6-7**). This suggests that the “resistance” module describes a
310 lineage-specific profile that can identify cells most likely to become refractory to AraC treatment.
311
312 The HL60-FLARE “resistance” module shared 9 genes with the C1498 “persistence” module:
313 ITSN1, VIM, CRIP1, S100A11, ANXA2, MYL6, S100A4, PSD3, and DOCK10. This set of genes
314 is highly active in cytoskeleton maintenance and remodeling. Such pathways are implicated in
315 the epithelial-to-mesenchymal transition (EMT), a type of transdifferentiation involved in cancer
316 cell migration, invasion, and drug resistance[35]. While EMT is less well studied in hematological
317 malignancies than solid tumors, there is increasing evidence of its relevance in diseases like
318 AML[36–40]. There was no significant correlation of module expression with any tested EMT gene
319 sets, suggesting that F1 module 1 and HL60 module 2 describe cell adhesion and motility
320 processes largely independent from canonical EMT (**Figure S4D**). The co-upregulation and
321 significant heritability of these genes in both cell lines under AraC treatment supports the pro-
322 survival role for cytoskeletal dynamics separate from EMT processes, potentially constituting a
323 form of CAM-DR. This is further supported by cell adhesion molecule genes present in the HL60
324 “resistance” module, including ITGB1, a primary mediator of CAM-DR[41] and LGALS1, implicated
325 in CAM-DR in multiple myeloma [42].
326
327 To identify whether heritable upregulation of CAM-DR genes in leukemic lineages prior to
328 treatment was associated with the generation of AraC resistance, we examined related
329 pathways in pre-experiment and control H1 cells. Sixty-five genes significantly upregulated in
330 treatment-naive H1 cells were also found in the HL60 population tree “resistance” module,
331 constituting an H1-specific pre-resistant state (**Figure S4E**).The majority of these genes are
332 also involved in cell motility and adhesion, such as NCAM1[43], PRICKLE1[44], BMP2[45], CPNE8[46],
333 and NAV3[47]. Also included are ANXA2 and PSD3, genes from the C1498 “persistence” module.
334 While H1 cells uniquely express this pre-resistant signature prior to AraC exposure, treatment
335 increased H1 population expression in a time-dependent manner (**Figure S4F**). In the control

336 setting, this signature does not clearly contribute to cell fitness, but under AraC, it confers a
337 large survival benefit.

338 Identification of pro-leukemic transcriptional programs associated with in 339 vivo immune escape

340 The mouse M1 “in vivo” module was the most heritable module over the F6 phylogenetic tree; it
341 showed significant enrichment in cells collected from M1 and may represent an in vivo
342 mechanism of survival through AraC treatment (**Figure 4A, S4G**). To determine shared
343 mechanisms with our HL60-FLARE modules, we again compared modules and found a strong
344 Jaccard index score between the M1 “in vivo” and our HL60-FLARE “resistance” modules
345 (**Table S10**, **Figures 4C, S4B-C**). These two modules share immunoproteasome genes
346 PSME1, PSME2, PSMB8, and PSMB9, immunoproteasome components involved in antigen
347 processing and presentation for MHC class I-mediated immune response. PSMB8 and PSMB9
348 encode two of the three beta core subunits of the 20S immunoproteasome core complex[48]. In a
349 variation of the immunoproteasome, the 20S core can complex with the 11S (or PA28ab)
350 regulatory cap, the primary subunits of which are encoded by the PSME1 (PA28a) and PSME2
351 (PA28b) genes[49]. There is evidence that peptide fragments produced by the 20S/11S
352 immunoproteasome may be less conducive to MHC class I presentation and lead to tumor cell
353 immune escape[50–52].
354
355 We investigated Psme1 and Psme2 expression patterns in F6 cells that survived engraftment
356 and treatment in our in vivo model. Differential gene expression analysis comparing F1 and F6
357 in vitro revealed universal F6-specific upregulation of 11S regulatory cap genes Psme1 and
358 Psme2 (**Table S2**). Additionally, Psmb8, Psme1, and Psme2 were significantly upregulated in
359 F6 clones in vivo compared to their in vitro counterparts proportional to clone success in vivo
360 (**Figures 4D, S4H**). F6 clones 1-5 upregulated Psme2 and Psmb8 in the in vivo setting,
361 representing a founder-specific enrichment. Expression of Psme1 differentiated F6 clones
362 further; significant in vivo upregulation was unique to clones F6.1, F6.2, and F6.4, the three
363 most successful clones in the blood (**Figures 4D, S3B**). While Psmb8 was significantly heritable
364 for F6 clones 1-5, Psme2 was only heritable in clones 1-3. In contrast, Psme1 expression was
365 only heritable over the lineage tree within clone F6.5. The evolutionary plasticity of Psme1
366 expression in the F6.1, F6.2, and F6.4 lineages may provide a competitive advantage within the
367 broader F6 immunoproteasome resistance mechanism.

Patient analysis

Phylogenetic reconstruction of in vitro and in vivo AraC-treated C1498-FLARE and HL60-FLARE cells revealed heritable gene modules associated with generating and maintaining AraC resistance. To validate their clinical relevance, we used gene expression data from the TARGET AML cohort (2,007 patients, ages 0-29), the most extensive, publicly available AML patient dataset[53]. The prognostic impact of module expression in bone marrow samples, collected at initial diagnosis, showed significantly increased hazard ratios associated with the expression of HL60-FLARE "resistance" module (HR 4.99), C1498-FLARE "persistence" module (HR 2.69), and "in vivo" module (HR 3.18) (**Figure 5A**). Kaplan Meier curves confirmed that heightened expression of these modules was associated with shorter overall survival (**Figure 5B-D**). These results support the ability of FLARE lineage tracing to generate heritability patterns relevant to AML patient survival.

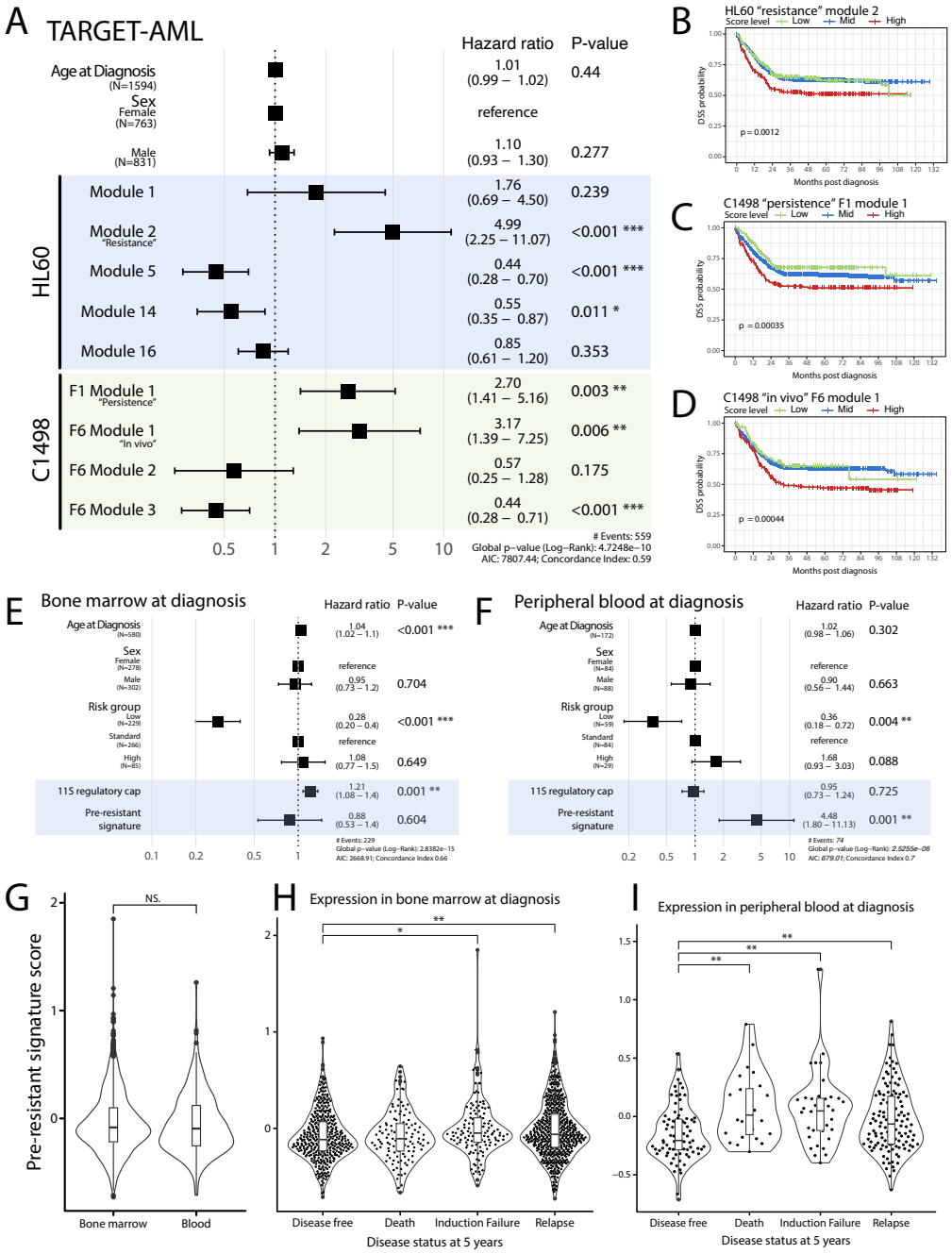

Figure 5: Expression levels of HL60-FLARE modules, C1498-FLARE modules, 11S regulatory cap genes, and pre-resistant signature genes are significantly associated with survival in pediatric AML patients. (**A**) Cox proportional hazard ratios for HL60-FLARE and C1498-FLARE Hotspot module scores calculated from bone marrow samples taken at diagnosis in the TARGET-AML cohort. (**B**) Kaplan Meier survival plots for the TARGET-AML cohort stratified into low, mid, and high expression of HL60-FLARE "resistance" module 2. Corresponding risk table can be found in supplementary table S11. (**C**) Kaplan Meier survival plots for the TARGET-AML cohort stratified into low, mid, and high expression of C1498-FLARE "persistence" F1 module 1. Corresponding risk table can be found in supplementary table S11. (**D**) Kaplan Meier survival plots for the TARGET-AML cohort stratified into low, mid, and high expression of C1498-FLARE "in vivo" F6 module 1. Corresponding risk table can be found in supplementary table S11. (**E**) Cox proportional hazard ratios for 11S regulatory cap and pre-resistant scores calculated from bone marrow samples taken at diagnosis in the TARGET-AML cohort. (**F**) Cox proportional hazard ratios for 11S regulatory cap and pre-resistant scores calculated from peripheral blood samples taken at diagnosis in the TARGET-AML cohort. (**G**) Violin plot showing pre-resistant signature scores calculated from samples taken at diagnosis. Bone marrow and blood samples do not significantly differ in signature scores. (**H**) Violin plot showing pre-resistant signature scores calculated from bone marrow samples taken at diagnosis. Mean scores for patients who experience induction failure or relapse within 5 years post diagnosis are minimally but significantly higher than patients who are disease free 5 years post diagnosis. Significance was calculated with Wilcoxon rank sum tests and Bonferroni corrected. (**I**) Violin plot showing pre-resistant signature scores calculated from peripheral blood samples taken at diagnosis. Mean scores for patients who experience death, induction failure, or relapse within 5 years post diagnosis are significantly higher than patients who are disease free 5 years post diagnosis. Significance was calculated with Wilcoxon rank sum tests and Bonferroni corrected.

We then focused on our pre-resistant/CAM-DR sub-module and 11S cap subunits of the 20S/11S immunoproteasome variant to explore their roles in treatment response and survival. We generated Cox proportional hazard ratios, including patient risk groups as covariates to account for interactions between risk group and signature expression. Expression levels of both signatures were associated with the risk of death independent of predefined risk groups. Interestingly, signature-associated risk of death differed drastically when patient expression scores were calculated from bone marrow or peripheral blood taken at diagnosis. In bone marrow samples, expression of 11S regulatory cap genes, but not the pre-resistant signature, was significantly associated with the risk of death (HR 1.21, p-value < 0.001, **Figure 5E**). Conversely, in peripheral blood, expression of the pre-resistant signature, but not the 11S regulatory cap genes, was significantly associated with a greater risk of death (HR 4.48, p-value < 0.001, **Figure 5F**). While 11S regulatory cap genes were expressed slightly more in bone marrow samples, potentially explaining why PSME1 and PSME2 expression have higher prognostic impact in bone marrow, there was no significant difference in expression of the pre-resistant sub-module between sample types (**Figure S5A, 5G**).

We then assessed the relationship between signature expression in pre-treatment diagnosis samples and patient status at 5 years post-inclusion. Specifically, we compared expression levels between patients who experienced death, induction failure, or relapse within 5 years compared to patients who remained disease-free for 5 years. Patients who experienced induction failure or relapse, but not death, tended to have higher pre-resistant sub-module scores in their blood and bone marrow samples at diagnosis (**Figure 5H-I**). Importantly, these trends were more dramatic when comparing blood samples at diagnosis; patients experiencing

induction failure, relapse, and death expressed significantly higher levels of the pre-resistant signature in blood compared to patients disease-free at 5 years. There was a slight negative relationship between pre-resistant sub-module score and peripheral blast percentage at diagnosis, suggesting this pattern does not reflect peripheral leukemic burden (**Figure S5B-C**).

Discussion

Chemotherapy resistance likely arises from the selection of pre-existing resistant populations and the reprogramming of previously sensitive cells. There is an unmet need for tools to dissect this evolution over time. We developed FLARE, a CRISPR-based dynamic lineage tracing system capable of tracking founder, clone, and subclone lineage in tandem with single-cell transcriptomics in response to chemotherapy. We demonstrated how our hierarchical approach can record cancer transcriptional evolution over an extended treatment time course, capturing both clonal evolution and selection of pre-existing cellular states. We used this technology to dissect the transcriptional evolution of AML, leveraging both in vitro and vivo systems and mouse and human models.

Using FLARE we uncovered the (1) heritable patterns of cell adhesion-associated AraC-tolerance and the (2) upregulation of immunoproteasome 11S regulatory cap subunits contributing to clone-specific in vivo fitness. The expression of both signatures in AML patients is significantly associated with shorter overall survival. High expression of PSME1 and PSME2, the major subunits of the 11S regulatory cap, in bone marrow but not peripheral blood, is associated with poorer prognosis. In contrast, high expression of our pre-resistant signature, which consists of various genes involved in cytoskeletal and cell adhesion pathways, is more informative when measured in blood samples taken at diagnosis. Both the 11S regulatory cap and pre-resistant signatures are composed of many genes not previously implicated in AML.

Our pre-resistant signature comprises many cell adhesion-mediated drug resistance (CAM-DR) genes. This mechanism has long been studied in the context of solid tumors, but its importance in hematological malignancies is growing[54,55]. Leukemic CAM-DR is thought to result from interactions between AML blasts and bone marrow stromal cells via various integrin molecules[56]. These interactions may protect leukemia cells, leading to minimum residual disease persistence and treatment failure upon disease recurrence[55]. This increased survival is thought to result from anoikis resistance, in which cells avoid apoptosis in response to becoming

457 detached from the extracellular matrix[57]. Interestingly, the emergence of CAM-DR in our work
458 was primarily seen in cells treated with AraC in standard in vitro cell culture. This may indicate
459 that treatment alone can lead to such resistance outside of the bone marrow niche.
460 Furthermore, survival analysis of the TARGET AML cohort revealed that expression of our
461 potential CAM-DR-associated pre-resistant signature had a significantly higher prognostic
462 impact when measured from peripheral blood samples taken at diagnosis. Our survival analysis
463 also suggests that the presence of leukemic blasts with enrichment of cytoskeletal, cell
464 adhesion, and cell motility processes in the blood before induction therapy is associated with
465 induction failure, death and relapse within 5 years of diagnosis. Therefore, patients with "pre-
466 resistant" lineages prior to treatment are less likely to benefit from induction chemotherapy, with
467 cells already displaying CAM-DR that can survive treatment and expand to outcompete other
468 leukemic lineages. This mechanism needs further exploration, but it suggests a secondary role
469 of CAM-DR in AML outside of the bone marrow niche.
470
471 While the exact pro-leukemic mechanism of our 11S signature cap is still unclear, there are data
472 to suggest the 11S regulatory cap leads to the generation of fewer peptides conducive to MHC
473 class I presentation and can interfere with tumor-specific epitope production[51,52,58]. 11S subunit
474 expression levels in pediatric AML patient bone marrow samples taken at diagnosis are
475 significantly associated with an increased risk of death and shorter overall survival. PSME1 and
476 PSME2 expression levels in bone marrow samples differed negligibly between patients with
477 adverse outcomes within 5 years compared to those that remained disease-free. This indicates
478 that while PSME1 and PSME2 expression in bone marrow is associated with a higher risk of
479 death, it is not highly predictive of induction failure or relapse within 5 years of diagnosis. It may
480 instead indicate the presence of leukemic lineages that are better able to evade immune
481 detection, resulting in a more aggressive and "colder" immune microenvironment.
482
483 In the future, the FLARE approach could be used to dissect the transcriptional evolution of other
484 tumor types under selective treatment pressure. Given the ability to sample tumor evolution
485 from tagged cell populations in circulating blood, this can be multiplexed to explore many more
486 initial cell states and treatment spaces. Moreover, this approach can be coupled to mouse
487 lineage-tracing models such as DARLIN[59] or the MARC1[60] mouse to capture the interplay
488 between engrafted tumor and immune cell populations in the context of checkpoint inhibitors
489 and other immunotherapies.

Methods

Cell Lines and drugs

The murine C1498 cell line (Cat# TIB-49) was purchased from ATCC in 2021. The HL60 AML cell line was a gift from Dr. Bonnie Lau's lab. C1498 cells were cultured in DMEM, supplemented with 10% FBS, 100 u/mL penicillin, and 100 ug/mL streptomycin. HL60 cells were cultured in Iscove's Modified Dulbecco's Medium, supplemented with 20% FBS, 100u/mL penicillin, and 100ug/mL streptomycin. All cell lines were expanded, aliquoted, and cryopreserved in culture media plus 5% DMSO and stored in liquid nitrogen upon receival. Active cell cultures were stored at 37°C with 5% CO_2. All cultured lines were regularly checked for the presence of mycoplasma using the Universal Mycoplasma Detection Kit (ATCC, 30-1012K). Cytarabine (AraC) powder was purchased from Selleck Chemicals (Cat # S1648). AraC was resuspended in PBS fresh for each in vitro and in vivo treatment.

Mice

KH2/iCas9 mice (Jackson Laboratory strain #029415) were a gift of the Huang lab at Dartmouth College. All mice were maintained in pathogen-free housing at the Center for Comparative Medicine and Research in Dartmouth Hitchcock Medical Center. All experimental protocols were approved by and performed in accordance with the guidelines of the Institutional Animal Care and Use Committee at Dartmouth College. To attenuate the immune response to Cas9, all injected KH2/iCas9 were exposed to doxycycline during in utero development through irradiated feed containing 625ppm doxycycline (ScottPharma, Inc. Marlborough, MA).

Molecular cloning

GESTALT lineage tracing system engineering

All digested vectors and fragments and PCR products were purified with the Monarch Gel Purification Kit (Cat# T1120S) or the Zymo Clean and Concentrate-5 Kit (Cat# D4003). All Gibson assembly reactions were conducted with NEB HiFi DNA Assembly 2x Master Mix (Cat# E2621S), following the ssDNA HiFi assembly protocol. Golden Gate assemblies were conducted following the Rice University Esp3I protocol. Chemical bacterial transformations were done with DH5alpha competent cells following the NEB Transformation Protocol with a 2-hour recovery at 37°C. Electroporated transformations were conducted with NEB Electrocompetent E. coli and were electroporated with the following conditions: 2kV, 200Ohms, 25uFd. All

520 bacterial cultures were grown in a 37°C shaker at 220-290rpm overnight. Vectors were purified
521 using either the Qiagen Miniprep Kit or the Zymo Midiprep II Kit. Correct cloning of all final
522 constructs was confirmed via Circuit-seq[61].

523 **FLARE-miniV10-10x-UMI**

524 Eight Cas9 target sequences were designed for high efficiency (>69% Doench) and low off
525 target scores. The eight-target array was purchased as a gene block from IDT, with upstream
526 Esp3I sites for founder tag insertion and NdeI + BamHI sites for cloning purposes. The target
527 gBlock and pLARRY-EGFP vector (Addgene #140025) were digested with NdeI+BamHI and
528 ligated together with Quick Ligase (Cat# M2200s). Resulting construct is referred to as
529 pLARRY-targets.
530
531 The PB-CMV-MCS-EF1-puro vector (Systems Bio cat #PB510B-1) was digested with SpeI and
532 HincII, removing the puromycin resistance gene, and then circularized with a Gibson assembly
533 reaction with a short single stranded joining oligo. The resulting construct is referred to as
534 miniPB.
535
536 The FLARE-miniV10-10x vector was then constructed by amplifying EGFP and the target array
537 from pLARRY-targets. The PCR primers used KpnI and EcoRI sites. The amplified
538 EGFP+target array and miniPB were digested with KpnI and EcoRI, gel purified, and ligated
539 together using T7 ligase. The 10X capture sequence 1 was incorporated via Gibson assembly.
540 The FLARE-miniV10-10x construct is available at Addgene (Plasmid #234492).
541
542 Founder tag oligos consisting of 14 degenerate bases (the founder tag) and Esp3I sites were
543 purchased from IDT. One cycle of PCR was used to anneal and extend the oligos. Founder tag
544 oligos were then inserted into FLARE-miniV10 via a Golden Gate Assembly reaction; the
545 resulting product is FLARE-miniV10-10X-UMI.

546 **FLARE-pbV10g-neo**

547 Individual Cas9 guides complementary to the target sequences in FLARE-miniV10 were
548 designed and cloned into the pX330-mCherry (Addgene #98750) vector using the Zheng Lab
549 pX330 cloning protocol. Guides, along with their individual U6 promoters, were amplified from
550 pX330-mCherry vectors. A secondary PCR reaction added flanking Esp3I sites to each U6-
551 guide fragment. Esp3I sites were also added to the PB-CMV-MCS-EF1-puro vector, while the
552 puro resistance gene was removed. U6/guide sequences were joined and inserted into PB-

553 CMV-MCS-EF1-puro via a 9-part Golden Gate Assembly reaction. The neomycin resistance
554 gene was amplified from the hCas9 vector and inserted into the U6/guide array vector via
555 Golden Gate Assembly. The FLARE-pbV10g-neo construct is available at Addgene (Plasmid
556 #234493).
557
558 In earlier versions of FLARE constructs, Cas9 guides were encoded into a single construct
559 along with the lineage recorder Cas9 target array. For reasons not yet fully understood, splitting
560 this into two vectors (FLARE-miniV10-10X and FLARE-pbV10g-neo) led to significantly higher
561 editing rates across targets.

562 **FLARE-pbCas9-tag-mCherry**
563 The miniPB construct was digested with KpnI for a Gibson Assembly insertion of a landing pad
564 containing a NotI and a new KpnI site. The resulting vector is referred to as miniPB-LP. The
565 pX330 construct was digested with KpnI and NotI to isolate the Cas9 transgene, which was then
566 ligated into the landing pad miniPB-LP vector. The resulting construct is referred to as miniPB-
567 Cas9.

568 The pX330-mCherry construct was digested with BamHI and HindIII for the insertion of a clone
569 tag landing pad containing type IIs restriction sites in the 3' UTR of the mCherry transgene using
570 Gibson Assembly. The mCherry transgene, including the clone tag landing pad, was amplified
571 and extended to include Gibson Assembly adaptors complementary to the insertion region in
572 miniPB-Cas9. The miniPB-Cas9 construct was then digested with NotI and the mCherry and
573 clone tag landing pad were inserted using Quick Ligase. The resulting construct is referred to as
574 FLARE-pbCas9-mCherry, and is available at Addgene (Plasmid #234494).

575 Lastly, clone tag oligos with Esp3I sites were purchased from IDT. For C1498-FLARE cells, the
576 clone tag consisted of 14 degenerate bases followed by 10x capture sequence 2. For HL60-
577 FLARE cells, the clone tag consisted of 38 patterned bases
578 (NNNWSNNNWSNNNWSNNNWSNNNWSNNNWSNNNWSNNNWSNNN, pattern from Johnson et al [62])
579 followed by 10x capture sequence 1. One cycle of PCR was used to anneal and extend the
580 oligos, and the resulting product was inserted into FLARE-pbCas9-mCherry via Golden Gate
581 Assembly. Capture sequence 2 was replaced by capture sequence 1 for HL60-FLARE cells due
582 to the planned discontinuation of support for capture sequence 2 announced by 10x.

583 ## Cell engineering and lineage tracing system testing

584 We used the Neon Electroporation System to integrate all piggyBac constructs into cells to
585 generate stable cell lines. Electroporations were carried out with the following protocols: C1498
586 cells were resuspended at 2x10^7 cells/mL and electroporated with 1080V, 50ms, and 1 pulse;
587 HL-60 cells were resuspended at 2x10^7 cells/mL and electroporated with 1450V, 35ms, and 1
588 pulse. All electroporations were done with the Neon 100ul tip system. Transposase:transposon
589 ratios for piggyBac integration ranged from 1:1 to 1:8. All FACS was conducted on a BD
590 FACSAria II or BD FACSAria Fusion. For antibiotic selection cells were incubated with selection
591 media for 1-3 weeks, and dead cells were removed from culture 2-3 times/week using a Ficoll
592 density gradient.
593
594 GESTALT constructs were introduced to cell lines in the following order: first low passage cells
595 were electroporated with FLARE-miniV10-10X-UMI and FLARE-pbV10g-neo. EGFP-positive
596 and neomycin resistant cells were isolated via FACS and 1ug/mL G418 selection. This step was
597 repeated two to three more times, gating for higher EGFP expression during FACS in each
598 subsequent round. For the third round of FACS for the C1498 cell line, individual cells were
599 sorted into wells of a 96-well plate to initiate individual clonal populations.
600
601 Prior to lineage tracing experiments, engineered lineage tracing cells were electroporated with
602 FLARE-pbCas9-tag-mCherry and mCherry+ cells were isolated via FACS. Cells were sorted
603 into bulk populations and 96-well plates at 100 cells/well.
604
605 Lineage recorder editing levels in C1498-FLARE cells over time were calculated using single
606 cell and bulk lineage barcode data. Day 0 editing was calculated from bulk (not a subset of
607 founders) C1498-FLARE cells prior to FLARE-pbCas9-tag-mCherry integration; day 13 editing
608 was calculated from this same population 13 days following integration post FACS. The
609 remaining editing rate timepoints were measured using the cell population used in C1498-
610 FLARE founder pool AraC treatment experiment and lineage recorder reads were subset for
611 reads containing valid founder tags associated with founders 1, 5, 6, and 11. Day 44 editing was
612 calculated from single cell sequencing of the founder pool subset for F1 and F6 prior to AraC
613 treatment. Day 64 editing was calculated from single cell sequencing of one untreated flask
614 cultured from the same population as used in day 44, and was subset for valid cells identified
615 via GEX analysis. Day 87 was also measured from one control flask from this population -
616 editing was calculated from single cell lineage endpoint data.

617 ## C1498-FLARE founder isolation and characterization

618 To screen individual C1498-FLARE founder populations for copies of FLARE-miniV10-10X-UMI
619 integrations gDNA was collected and founder tags were amplified and prepared into sequencing
620 libraries. Founder tag libraries for individual populations were multiplexed and sequenced on an
621 Illumina MiniSeq with a Mid-Ouput 300-cycle kit. Founder tags for each clone were determined
622 as having > 4,300 reads. Cells from each clone were expanded, aliquoted, and cryopreserved.

623 **Growth curves**

624 To begin growth curves for individual founders, cells were resuspended at 50k cells/mL and
625 plated in T25 flasks in triplicate. From day 0-7, two 10ul aliquots from each flask were mixed
626 with 10ul Trypan Blue and counted on the Luna II Cell Counter daily. Growth curve data were
627 analyzed and plotting using the Growthcurver R package [63].

628 **AraC dose-response curves**

629 Cells were plated at 15,000 cells/well in a 96-well plate in media containing various AraC
630 dosages in triplicate (0.0001mg/ml-10mg/ml). 100ul of CellTiter 96 AQueous One Solution (Cat#
631 G3582) was added to each well and after incubation for 1-3 hours absorbance was measured at
632 490nm on a SpectraMax i3x. Absorbance from wells containing media without cells or drug
633 were averaged to calculate background absorbance. Corrected absorbance for each well was
634 calculated as (well absorbance - background absorbance). Corrected absorbances were then
635 loaded into the drc R package for generating dose-response curves, ED50 values, and EC50
636 values[64].

637 **Whole genome sequencing**

638 High molecular weight (HMW) gDNA was isolated from parental C1498 cells and individually
639 engineered clones using the Monarch High Molecular Weight gDNA Kit for Cells (Cat# T3050S).
640 HMW gDNA samples were multiplexed and prepared into a sequencing library following the
641 Oxford Nanopore SQK-NBD114.24 kit. The library was then sequenced on a PromethION flow
642 cell with R10.4.1 chemistry. Sequencing data were basecalled and demultiplexed using Guppy.
643 Variants were called using PEPPER-Margin-DeepVariant, SNPs were isolated and filtered for a
644 minimum quality of 20 and mean depth between 10 and 80. To remove population variants, the
645 GRCm39 dbSNP was annotated using Ensembl VEP and variants with moderate or high impact
646 were removed. The resulting dbSNP was subtracted from filtered SNPs using Bedtools [65].
647 Remaining variants were annotated with Ensembl VEP and intersected with datasets of known
648 AML mutations.

649 ## AraC response and resistance experiments

650 **C1498-FLARE founder pool treatment response and resistance**

651 C1498-FLARE founders F1, F5, F6, and F11 were sorted by FACS on day 13 following
652 electroporation with the FLARE-pbCas9-tag-mCherry vector. Cells were sorted into 96-well
653 plates at 100 cells/well. In vitro AraC treatment began on day 44 (31 days post FACS). Cells
654 were allowed to grow for a longer period following sorting due to growth rate differences
655 between founders. On day 44, 1 well of sorted cells for each clone was pooled at equal
656 numbers and split into four flasks for in vitro treatment with an aliquot set aside for mouse
657 injections.

658 *In vitro*

659 Two flasks were maintained in normal culture media, the remaining two flasks were maintained
660 in media containing 0.05ug/ml AraC. Flasks were maintained for 43 days to allow for the
661 development of AraC resistance. Media was replaced 2-3 times/week and split when needed.
662 Dose-response curves were calculated for each flask on day 15 of treatment, and a final dose-
663 response curve was calculated for flask displaying resistance on day 36 of treatment. On day 43
664 of treatment, cells were prepared for MULTIseq tagging and single cell capture following
665 MULTIseq and 10x protocols.

666 *In vivo*

667 Pooled C1498 clone cells were washed twice with PBS, resuspended at 250,000 cells/mL and
668 filtered through a 40uM filter. Mice were injected IV with 100ul of cell suspension (25,000
669 cells/mouse). On day 14 mice were randomly assigned to treatment groups; on days 14-16
670 treatment mice received 100mg/kg AraC IP and control mice received an equal volume of PBS.
671 Blood was collected via the retro-orbital sinus on days 13, 28, 43, 50, and 57. Prior to blood
672 draws mice were anesthetized with Isoflurane. Microhematocrit capillary tubes were placed in
673 1.7mL tubes containing 50mM EDTA and then used to collect 50-200ul of blood from the retro-
674 orbital sinus into EDTA coated tubes. Blood samples were then kept on ice until further
675 processing. Mice displaying symptoms of high AML burden were euthanized. All surviving mice
676 were euthanized on day 67 post cell injections. Upon euthanasia whole blood was collected via
677 cardiac puncture and femoral bone marrow was harvested. gDNA was isolated from 20ul of
678 whole blood, and remaining blood was separated using a Ficoll-paque density gradient to
679 isolate PBMCs. To isolate bone marrow, 18g needles were used to puncture the bottom of
680 0.5mL tubes, femur bones were placed in the 0.5mL tubes and nested in 1.7mL tubes, and

681 tubes were spun at > 10,000g for 20 seconds. Bone marrow pellets and PBMCs were methanol
682 fixed and permeabilized following 10x protocols.

683 **Human AML cell line in vitro treatment response**

684 Engineered lineage tracing HL60-FLARE cells were sorted into 96-well plates at 100 cells/well
685 following electroporation with FLARE-pbCas9-tag-mCherry to establish GESTALT lineage
686 tracing populations, as described above. Sorted well populations were expanded for 23 days.
687 On day 23 post FACS, five expanded wells were combined into an initial cell pool. The pool was
688 then split for 10x scRNA-seq preparation, methanol fixation, cryopreservation, and in vitro AraC
689 treatment. For in vitro AraC treatment cell pools were split into control (no AraC) and AraC
690 conditions (0.01ug/mL AraC). All treatment wells were cultured in duplicates. AraC solutions and
691 media were made fresh for media changes twice per week, and wells were split as needed. Cell
692 concentration for each well was measured once per week in duplicates using the Luna II Cell
693 Counter. Cells were regularly cryopreserved through the experiment for later analysis. In vitro
694 treatment continued for 89 days, after which cells were prepared for 10x scRNA-seq preparation
695 with MULTIseq multiplexing.

696 Lineage library preparation and sequencing

697 All PCR reactions were conducted using Q5 HotStart Polymerase (Cat # M0494L) and Sybr
698 Green dye. DNA was purified from PCR reactions using Omega TotalPure NGS magnetic
699 beads with 0.8-1.5x ratios based on amplicon size.

700 **Bulk DNA library preparation and sequencing**

701 gDNA was collected from cultured cells, PBMCs, and bone marrow samples using the Qiagen
702 DNeasy Blood and Tissue Kit (Cat# 69504). For library preparation, lineage recorders (including
703 founder tags and clone tags) were first tagged with sequencing UMIs prior to amplification to
704 control for PCR bias, with the exception of libraries constructed from blood collections. Blood
705 collection libraries were treated as sensitive samples, as C1498-FLARE cells were sparse in the
706 blood. As a result, these libraries were amplified without sequencing UMIs and initial PCRs were
707 set up in a PCR hood to prevent contamination. For all libraries, TruSeq/Nextera indices and
708 Illumina adaptors were subsequently attached with PCR. Final sequencing libraries were
709 quantified with the Qubit fluorometer and the NEB NextQuant Library Quant kit (Cat # E7630L).
710 Libraries were then diluted to the appropriate loading concentration for sequencing.

711 **Single cell library preparation and sequencing**

712 Cells were captured for single cell sequencing following 10x guidelines for 3' scRNA-seq with
713 feature barcoding. For multiplexed single cell experiments, cells were first tagged following
714 MULTIseq protocols (Millipore Sigma, LMO001)[66]. Gene expression and MULTIseq libraries
715 were constructed and quantified following 10x and MULTIseq guidelines with one alteration - a
716 portion of cDNA was set aside following initial cDNA amplification but prior to SPRIselect
717 cleanup to be used for FLARE lineage library construction. This was done to avoid splitting
718 FLARE transcripts between GEX and feature barcoding fractions.

719 The previously set aside cDNA was purified using a 2x bead cleanup. For each sample, cDNA
720 was split to generate a library of dynamic lineage recorders (which includes founder tags) and a
721 library of clone tags. All single cell FLARE libraries were initially amplified in 9-16 replicate wells
722 and then combined into 3-4 separate sub-libraries. TruSeq/Nextera indices and Illumina
723 adaptors were subsequently attached with PCR. Final sequencing libraries were quantified with
724 the Qubit fluorometer and the NEB NextQuant Library Quant kit (Cat # E7630L). Libraries were
725 then diluted to the appropriate loading concentration for sequencing.

726 Computational analysis

727 **Sequencing data pre-processing**

728 For bulk DNA sequencing raw data were converted to fastq format using bcl2fastq2 or BCL
729 Convert (Illumina). For single cell RNA sequencing raw data were converted to fastq format
730 using CellRanger mkfastq. Cells were then called using CellRanger count for non-multiplexed
731 10x runs or CellRanger multi for MULTIseq multiplexed 10x runs[67].

732 **Single cell RNA-seq analysis**

733 Cellranger output filtered matrices were analyzed with Seurat 5.1.0[68]. Low quality cells were
734 filtered out based on the number of RNA features and percentage of mitochondrial reads. For
735 non-multiplexed samples doublets were identified and removed using the scDblFinder R
736 package[69]. For multiplexed samples, MULTIseq barcode filtered matrices were added as Assay
737 Objects to Seurat objects. Cells were demultiplexed and doublets were identified and removed
738 with the *MULTIseqDemux()* function. For PBMC and bone marrow samples cell type
739 annotations were added using the SingleR R package with the MouseRNAseqData reference
740 set from the celldex R package[70]. All single cell Seurat objects were normalized with the
741 SCTransform R package for data visualization and integration with other objects[71,72]. Differential

742 gene expression analysis was conducted using the *FindMarkers()* and *FindAllMarkers()* Seurat
743 functions.

744 **Gene set enrichment analysis**

745 C1498-FLARE founder-specific gene set enrichment analysis was conducted with the fGSEA R
746 package[73]. Differentially expressed genes were identified for each founder by Wilcoxon rank
747 sum test and input into the fGSEA function with Mus musculus Hallmark gene sets from
748 mSigDB.

749 **Single cell lineage analysis and tree reconstruction**

750 *Founder and clone tag clustering*

751 To map founder tags to founder tag groups (or founders) and clone tags to clone tag groups (or
752 clones), we used a clustering strategy based on per cell tag set similarity. Briefly, given a
753 mapping of cells to a set of tags, a graph was constructed with cells as nodes and Jaccard
754 similarity as edges. Jaccard similarity was calculated pairwise as the intersection between per
755 cell tag sets divided by the union of per cell tag sets. Any pairs of cells with a Jaccard similarity
756 of 0 (indicating no overlapping tags) shared no edges. Cells were assigned to clusters using the
757 Louvain algorithm for community detection which returned the partition that maximized
758 modularity and with resolution = 1.

759 *Founder assignment*

760 To extract lineage information from scRNA-seq-captured dynamic lineage recorders, we first
761 used SingleCellLineage, as previously described[13,14]. Briefly, sequences are collapsed by 10x
762 UMI and aligned to the reference to obtain a pattern of insertions and deletions across a target
763 array per cell. Founder tags, located immediately upstream of the lineage recorders, were
764 extracted per collapsed merged read. We filtered cell barcodes against the 10x feature
765 barcoding Cell ID whitelist. Merged reads with less than 85% identity to the reference sequence
766 were removed from the dataset. To ensure we were using high quality barcodes to build single-
767 cell lineage trees, we leveraged tools from the Cassiopeia pipeline[74] to perform additional data
768 cleaning. Founder tags were corrected for PCR errors via Starcode[75] with Levenshtein distance
769 = 1. UMIs were error corrected using Cassiopeia function *error_correct_umi()*. Finally, we
770 filtered our error corrected founder tags and target arrays using *filter_molecule_table()* to
771 remove low read count UMIs and cells with too few UMIs. Additionally, this step ensures there is
772 only one target array per 10x cell ID-founder tag combination.
773

774 Founders were assigned by the combination of founder tag integrations in cells. For C1498-
775 FLARE founder populations, founder tag assignments were previously determined via sub-
776 founder culturing and bulk gDNA sequencing. Therefore, if cells had reads mapping to more
777 than one founder based on the founder tags found in its lineage data, it was assigned to a
778 founder based on the total sum of reads and UMIs associated with a certain founder group.
779 Only cells with 90% identity to a certain founder were kept.
780
781 Unlike the C1498-FLARE founders, HL60-FLARE founders had no ground truth mapping of
782 founder tags to founder groups. Subsequently, we took additional steps to ensure we had a
783 confident list of founder tags per cell and group. To remove within-cell background noise, we
784 removed integrations that made up less than 1.5% of reads per cell. This threshold was based
785 on qualitative inspection of the distribution of integration read counts per integration per cell.
786 The founder tags were further filtered by removing tags found in fewer than 5 cells across the
787 dataset. The cleaned set of tags were clustered into founders as described previously (*Founder*
788 *and clone tag clustering*). Finally, to refine the final set of founder tags defining a founder, we
789 filtered for tags with greater than 50% identity to a single founder group. This threshold was
790 based on visual inspection of the distribution of tag identity to founders, determined by the total
791 number of cells with a tag in a founder divided by the total number of cells with a tag. This
792 additionally ensures that each founder tag is found in one founder.

793 *Clone assignment*
794 Clone tags were extracted from sequencing reads using the SingleCellLineage pipeline. For
795 HL60-FLARE clone tag reads, only tags matching the expected 38bp IUPAC pattern were kept.
796 Clone tag reads with more than one missing base within the tag sequence window were
797 removed from the dataset, then clone tags were error corrected using Starcode with
798 Levenshtein distance = 1 for 14 bp tags or Levenshtein distance = 2 for 38 bp tags. These clone
799 tags were then filtered for read count > 1 and number of UMIs > 1. Tags with nucleotide repeats
800 of 5 or longer were also removed (i.e. AAAAA, TTTTT, GGGGG, CCCCC). Background tags,
801 defined as contributing to fewer than 10% of all reads in the cell, were filtered out. Finally, clone
802 tags were discretized to founders by keeping tags with 90% identity (C1498s, 2 founders) or
803 50% identity (HL60s, 15 founders) to a given founder based on the total proportion of reads per
804 clone tags. C1498-FLARE and HL60-FLARE cells were assigned to clones as previously
805 described (*Founder and clone tag clustering*) given the final set of clone tags.

806 *Building Trees*

807 Trees were reconstructed per clone using Cassiopeia's[74] greedy vanilla solver from the pattern
808 of indels per target array. The method was chosen for its scalability given the size of our trees
809 ranges from tens to thousands of cells. Briefly, a tree is built in a top-down fashion by splitting
810 cells into two groups based on the most frequent mutation in the population. Cell subsets are
811 repeatedly split until only one cell remains per subset. Clones belonging to the same founder
812 population were combined into founder trees using a custom python script to attach trees at the
813 root, due to the hierarchical nature of the lineage tracing tag system. All founder trees were
814 combined with the same method to generate a population tree. Cells with unedited/wildtype
815 target arrays were removed from the analysis prior to building the trees.

816 *PATH analysis*
817 To identify genes that were significantly heritable in our clonal population we used the recently
818 published tool, PATH [28]. PATH takes as input a phylogenetic tree along with either discrete
819 annotations like cluster assignments or continuous data like gene expression or module scores.
820 We considered the top 3000 highly variable features per tree to identify genes with strong
821 autocorrelations, suggesting high heritability.

822 *Hotspot module generation*
823 To identify informative gene expression modules based on our single-cell lineage trees and
824 gene expression data, we leveraged the tool Hotspot[34] as described in the following vignette
825 https://hotspot.readthedocs.io/en/latest/Lineage_Tutorial.html. Briefly, we ran Hotspot on our
826 log-normalized data via the 'normal' model filtered for genes in a minimum of 10 cells. Then we
827 generated the KNN graph with 10 neighbors. Autocorrelation scores are calculated per gene to
828 perform feature selection. These genes are then correlated to generate a gene-by-gene matrix,
829 which is used to identify modules using a hierarchical clustering approach with
830 min_gene_threshold = 10 to control the size of modules being joined.

831 *Module overlap analysis*
832 C1498-FLARE module mouse genes were converted to human orthologs for analysis. C1498-
833 FLARE and HL60-FLARE modules were assessed for significant overlap as measured by
834 Jaccard indices and odds ratios compared to genomic background using the GeneOverlap R
835 package[76].

836 **Survival analysis**

837 TARGET-AML RNAseq, clinical, and sample data were accessed through the cBioPortal.
838 Expression datasets were split by sample type where applicable. Sample expression scores for
839 modules and gene sets were calculated by averaging the FPKM or RPKM scores. Cox
840 proportional hazard ratios were generated using the survival R package[77]. To stratify patients for
841 Kaplan-Meier analysis, we first determined the expression score mean and standard deviation
842 within the samples of interest. Patients with scores within one standard deviation of the mean
843 were assigned to the Mid-expression group. Patients with scores above and below one standard
844 deviation of the mean were assigned to the High and Low expression groups, respectively. We
845 excluded patient samples missing information for tissue type.

846 Acknowledgments

847 We thank the members of the McKenna lab for experimental help and scientific input. We
848 especially thank Aidan Cook for his computational expertise. In addition, we thank Prerna
849 Malaney and Bonnie Lau for their expertise in AML, and Brock Christensen for his input on
850 survival analyses. We acknowledge the Dartmouth Cancer Center and the shared resources
851 supported by NCI Cancer Center Support Grant 5P30CA023108. We especially thank Fred W.
852 Kolling IV, Laurent Perreard, and Carol Ringelberg of the GMBSR for their sequencing guidance
853 and expertise. FACS was carried out by Gary Ward in DartLab, the Immune Monitoring and
854 Flow Cytometry Shared Resource at the Dartmouth Cancer Center (RRID: SCR_019165). We
855 also acknowledge the Dartmouth Cancer Center Irradiation, Imaging, Microscopy, and Animal
856 Cancer Models Shared Resource (RRID:SCR_023478), and specifically Jennifer Fields for her
857 help with animal experiment strategy. All Illumina sequencing was carried out in the Genomics
858 and Molecular Biology Shared Resource (RRID:SCR_021293) which is additionally supported
859 by NIH S10 (1S10OD030242) awards. Single-cell studies were conducted through the
860 Dartmouth Center for Quantitative Biology in collaboration with the GMBSR with support from
861 NIGMS COBRE (P20GM130454) and NIH S10 (S10OD025235) awards. This work was
862 supported by DP2GM149750 and the V Foundation, and A.M. is supported by The Pew
863 Biomedical Scholars program.

864 Data availability

865 All sequencing data associated with this publication have been deposited in NCBI's Gene
866 Expression Omnibus[78] and are accessible through GEO Series accession numbers GSE289454
867 and GSE289459.

References

1. Boyd, A. L. *et al.* Identification of Chemotherapy-Induced Leukemic-Regenerating Cells Reveals a Transient Vulnerability of Human AML Recurrence. *Cancer Cell* **34**, 483-498.e5 (2018).
2. Stetson, L. C. *et al.* Single cell RNA sequencing of AML initiating cells reveals RNA-based evolution during disease progression. *Leukemia* **35**, 2799–2812 (2021).
3. Morita, K. *et al.* Clonal evolution of acute myeloid leukemia revealed by high-throughput single-cell genomics. *Nature Communications 2020 11:1* **11**, 1–17 (2020).
4. Ojamies, P. N. *et al.* Monitoring therapy responses at the leukemic subclone level by ultra-deep amplicon resequencing in acute myeloid leukemia. *Leukemia 2017 31:5* **31**, 1048–1058 (2016).
5. Docking, T. R. *et al.* A clinical transcriptome approach to patient stratification and therapy selection in acute myeloid leukemia. *Nat. Commun.* **12**, 2474 (2021).
6. Severens, J. F. *et al.* Mapping AML heterogeneity - multi-cohort transcriptomic analysis identifies novel clusters and divergent ex-vivo drug responses. *Leukemia* **38**, 751–761 (2024).
7. Stratmann, S. *et al.* Transcriptomic analysis reveals proinflammatory signatures associated with acute myeloid leukemia progression. *Blood Adv.* **6**, 152–164 (2022).
8. Thol, F. & Ganser, A. Treatment of Relapsed Acute Myeloid Leukemia. *Current Treatment Options in Oncology* vol. 21 Preprint at https://doi.org/10.1007/s11864-020-00765-5 (2020).
9. Yan, B. *et al.* Low-frequency TP53 hotspot mutation contributes to chemoresistance through clonal expansion in acute myeloid leukemia. *Leukemia* **34**, 1816–1827 (2020).
10. Sharma, S. V. *et al.* A Chromatin-Mediated Reversible Drug-Tolerant State in Cancer Cell Subpopulations. *Cell* **141**, 69–80 (2010).
11. Shaffer, S. M. *et al.* Rare cell variability and drug-induced reprogramming as a mode of cancer drug resistance. *Nature* **546**, 431–435 (2017).
12. Caiado, F. *et al.* Lineage tracing of acute myeloid leukemia reveals the impact of hypomethylating agents on chemoresistance selection. *Nat. Commun.* **10**, 1–15 (2019).
13. McKenna, A. *et al.* Whole-organism lineage tracing by combinatorial and cumulative genome editing. *Science* **353**, aaf7907 (2016).
14. Simeonov, K., Mckenna, A., Shendure, J. & Legner, C. Single-cell lineage and transcriptome reconstruction of metastatic cancer reveals selection of aggressive hybrid EMT states. 1–36 (2020).

901 15. Quinn, J. J. *et al.* Continuous lineage recording reveals rapid, multidirectional metastasis in
902 a lung cancer xenograft model in mouse. *bioRxiv* 2020.04.16.045245 (2020).
903 16. Driss, V. *et al.* Sub-clonal analysis of the murine C1498 acute myeloid leukaemia cell line
904 reveals genomic and immunogenic diversity. *Immunol. Lett.* **192**, 27–34 (2017).
905 17. de la Cruz López, K. G., Toledo Guzmán, M. E., Sánchez, E. O. & García Carrancá, A.
906 MTORC1 as a regulator of mitochondrial functions and a therapeutic target in cancer.
907 *Front. Oncol.* **9**, 1373 (2019).
908 18. Zeng, Z. *et al.* Targeting of mTORC1/2 by the mTOR kinase inhibitor PP242 induces
909 apoptosis in AML cells under conditions mimicking the bone marrow microenvironment.
910 *Blood* **120**, 2679–2689 (2012).
911 19. Schulze, A., Oshi, M., Endo, I. & Takabe, K. MYC targets scores are associated with
912 cancer aggressiveness and poor survival in ER-positive primary and metastatic breast
913 cancer. *Int. J. Mol. Sci.* **21**, 8127 (2020).
914 20. Donati, G. *et al.* Targeting mitochondrial respiration and the BCL2 family in high-grade
915 MYC-associated B-cell lymphoma. *Mol. Oncol.* **16**, 1132–1152 (2022).
916 21. Quan, Q., Xiong, X., Wu, S. & Yu, M. Identification of immune-related key genes in Ovarian
917 Cancer based on WGCNA. *Front. Genet.* **12**, 760225 (2021).
918 22. Xiao, X.-Y. *et al.* TRAT1 overexpression delays cancer progression and is associated with
919 immune infiltration in lung adenocarcinoma. *Front. Oncol.* **12**, 960866 (2022).
920 23. Lee, H. *et al.* A novel immune prognostic index for stratification of high-risk patients with
921 early breast cancer. *Sci. Rep.* **11**, 128 (2021).
922 24. Xie, W. *et al.* Identification of low-density lipoprotein receptor class A domain containing 4
923 (LDLRAD4) as a prognostic indicator in primary gastrointestinal stromal tumors. *Curr.*
924 *Probl. Cancer* **44**, 100593 (2020).
925 25. Liu, Z. *et al.* Low density lipoprotein receptor class A domain containing 4 (LDLRAD4)
926 promotes tumorigenesis of hepatic cancer cells. *Exp. Cell Res.* **360**, 189–198 (2017).
927 26. Ou, R. *et al.* Transcriptome analysis of CD34+ cells from myelodysplastic syndrome
928 patients. *Leuk. Res.* **62**, 40–50 (2017).
929 27. Bowling, S. *et al.* An engineered CRISPR/Cas9 mouse line for simultaneous readout of
930 lineage histories and gene expression profiles in single cells. *Cell* **181**, 1410 (2020).
931 28. Schiffman, J. S. *et al.* Defining heritability, plasticity, and transition dynamics of cellular
932 phenotypes in somatic evolution. *Nat. Genet.* **56**, 2174–2184 (2024).
933 29. Park, S. *et al.* Genome-wide genotype-based risk model for survival in core binding factor
934 acute myeloid leukemia patients. *Ann. Hematol.* **97**, 955–965 (2018).

935 30. Venditti, A. *et al.* Prognostic relevance of the expression of Tdt and CD7 in 335 cases of
936 acute myeloid leukemia. *Leukemia* **12**, 1056–1063 (1998).
937 31. Saxena, A. *et al.* Biologic and clinical significance of CD7 expression in acute myeloid
938 leukemia. *Am. J. Hematol.* **58**, 278–284 (1998).
939 32. Ogata, K. *et al.* Reappraisal of the clinical significance of CD7 expression in association
940 with cytogenetics in de novo acute myeloid leukaemia: Short Report. *Br. J. Haematol.* **115**,
941 612–615 (2001).
942 33. Dalton, W. T., Jr *et al.* HL-60 cell line was derived from a patient with FAB-M2 and not
943 FAB-M3. *Blood* **71**, 242–247 (1988).
944 34. DeTomaso, D. & Yosef, N. Hotspot identifies informative gene modules across modalities
945 of single-cell genomics. *Cell Syst.* **12**, 446-456.e9 (2021).
946 35. Ribatti, D., Tamma, R. & Annese, T. Epithelial-mesenchymal transition in cancer: A
947 historical overview. *Transl. Oncol.* **13**, 100773 (2020).
948 36. Wu, S., Du, Y., Beckford, J. & Alachkar, H. Upregulation of the EMT marker vimentin is
949 associated with poor clinical outcome in acute myeloid leukemia. *J. Transl. Med.* **16**, 170
950 (2018).
951 37. Varisli, L. & Vlahopoulos, S. Epithelial-mesenchymal transition in acute leukemias. *Int. J.*
952 *Mol. Sci.* **25**, 2173 (2024).
953 38. Greaves, D. & Calle, Y. Epithelial mesenchymal transition (EMT) and associated invasive
954 adhesions in solid and haematological tumours. *Cells* **11**, 649 (2022).
955 39. Cuevas, D. *et al.* The role of epithelial-to-mesenchymal transition transcription factors
956 (EMT-TFs) in acute myeloid leukemia progression. *Biomedicines* **12**, 1915 (2024).
957 40. Qi, J. *et al.* Five EMT-Related Gene Signatures Predict Acute Myeloid Leukemia Patient
958 Outcome. *Disease Markers* **2022**, 1–8 (2022).
959 41. Damiano, J. S., Hazlehurst, L. A. & Dalton, W. S. Cell adhesion-mediated drug resistance
960 (CAM-DR) protects the K562 chronic myelogenous leukemia cell line from apoptosis
961 induced by BCR/ABL inhibition, cytotoxic drugs, and gamma-irradiation. *Leukemia* **15**,
962 1232–1239 (2001).
963 42. Hu, Q., Wang, M., Wang, J., Tao, Y. & Niu, T. Development of a cell adhesion-based
964 prognostic model for multiple myeloma: Insights into chemotherapy response and potential
965 reversal of adhesion effects. *Oncol. Res.* **32**, 753–768 (2024).
966 43. Sasca, D. *et al.* NCAM1 (CD56) promotes leukemogenesis and confers drug resistance in
967 AML. *Blood* **133**, 2305–2319 (2019).

968 44. Lim, B. C. *et al.* Prickle1 promotes focal adhesion disassembly in cooperation with the
969 CLASP-LL5β complex in migrating cells. *J. Cell Sci.* **129**, 3115–3129 (2016).
970 45. Jin, H. *et al.* BMP2 promotes migration and invasion of breast cancer cells via cytoskeletal
971 reorganization and adhesion decrease: an AFM investigation. *Appl. Microbiol. Biotechnol.*
972 **93**, 1715–1723 (2012).
973 46. Zhang, P. *et al.* CPNE8 promotes gastric cancer metastasis by modulating focal adhesion
974 pathway and tumor microenvironment. *Int. J. Biol. Sci.* **18**, 4932–4949 (2022).
975 47. Škarková, A. *et al.* Microtubule-associated NAV3 regulates invasive phenotypes in
976 glioblastoma cells. *Brain Pathol.* **35**, e13294 (2025).
977 48. Csizmar, C. M., Kim, D.-H. & Sachs, Z. The role of the proteasome in AML. *Blood Cancer*
978 *J.* **6**, e503 (2016).
979 49. Groettrup, M. *et al.* The interferon-gamma-inducible 11 S regulator (PA28) and the
980 LMP2/LMP7 subunits govern the peptide production by the 20 S proteasome in vitro. *J.*
981 *Biol. Chem.* **270**, 23808–23815 (1995).
982 50. Seliger, B., Cabrera, T., Garrido, F. & Ferrone, S. HLA class I antigen abnormalities and
983 immune escape by malignant cells. *Semin. Cancer Biol.* **12**, 3–13 (2002).
984 51. Kurnick, J. T. *et al.* A novel autocrine pathway of tumor escape from immune recognition:
985 melanoma cell lines produce a soluble protein that diminishes expression of the gene
986 encoding the melanocyte lineage melan-A/MART-1 antigen through down-modulation of its
987 promoter. *J. Immunol.* **167**, 1204–1211 (2001).
988 52. Raule, M. *et al.* PA28αβ reduces size and increases hydrophilicity of 20S
989 immunoproteasome peptide products. *Chem. Biol.* **21**, 470–480 (2014).
990 53. Farrar, J. E. *et al.* Genomic profiling of pediatric acute myeloid leukemia reveals a changing
991 mutational landscape from disease diagnosis to relapse. *Cancer Res.* **76**, 2197–2205
992 (2016).
993 54. Kim, H. N., Ruan, Y., Ogana, H. & Kim, Y.-M. Cadherins, selectins, and integrins in CAM-
994 DR in leukemia. *Front. Oncol.* **10**, 592733 (2020).
995 55. Chen, W.-C., Hu, G. & Hazlehurst, L. A. Contribution of the bone marrow stromal cells in
996 mediating drug resistance in hematopoietic tumors. *Curr. Opin. Pharmacol.* **54**, 36–43
997 (2020).
998 56. Kuželová, K., Obr, A., Marková, J. & Gašová, Z. Integrin expression and adhesivity to
999 fibronectin in primary acute myeloid leukemia cells: Impact of NPM1 and FLT3 mutations.
1000 *Eur. J. Haematol.* **105**, 578–587 (2020).

1001 57. Estrugo, D. *et al.* Ligand bound beta1 integrins inhibit procaspase-8 for mediating cell
1002 adhesion-mediated drug and radiation resistance in human leukemia cells. *PLoS One* **2**,
1003 e269 (2007).
1004 58. Keller, M. *et al.* The proteasome immunosubunits, PA28 and ER-aminopeptidase 1 protect
1005 melanoma cells from efficient MART-126-35 -specific T-cell recognition: Antigen
1006 processing. *Eur. J. Immunol.* **45**, 3257–3268 (2015).
1007 59. Li, L. *et al.* A mouse model with high clonal barcode diversity for joint lineage,
1008 transcriptomic, and epigenomic profiling in single cells. *Cell* **186**, 5183-5199.e22 (2023).
1009 60. Kalhor, R. *et al.* Developmental barcoding of whole mouse via homing CRISPR. *Science*
1010 **361**, eaat9804 (2018).
1011 61. Emiliani, F. E., Hsu, I. & McKenna, A. Multiplexed assembly and annotation of synthetic
1012 biology constructs using long-read nanopore sequencing. *ACS Synth. Biol.* **11**, 2238–2246
1013 (2022).
1014 62. Johnson, M. S., Venkataram, S. & Kryazhimskiy, S. Best Practices in Designing,
1015 Sequencing, and Identifying Random DNA Barcodes. *J. Mol. Evol.* **91**, 263–280 (2023).
1016 63. Sprouffske, K. Simple Metrics to Summarize Growth Curves [R package growthcurver
1017 version 0.3.1]. (2020).
1018 64. Ritz, C., Baty, F., Streibig, J. C. & Gerhard, D. Dose-Response Analysis Using R. *PLoS*
1019 *One* **10**, e0146021 (2015).
1020 65. Quinlan, A. R. & Hall, I. M. BEDTools: a flexible suite of utilities for comparing genomic
1021 features. *Bioinformatics* **26**, 841–842 (2010).
1022 66. McGinnis, C. S. *et al.* MULTI-seq: sample multiplexing for single-cell RNA sequencing
1023 using lipid-tagged indices. *Nature Methods 2019 16:7* **16**, 619–626 (2019).
1024 67. Zheng, G. X. Y. *et al.* Massively parallel digital transcriptional profiling of single cells. *Nat.*
1025 *Commun.* **8**, 14049 (2017).
1026 68. Hao, Y. *et al.* Dictionary learning for integrative, multimodal and scalable single-cell
1027 analysis. *Nat. Biotechnol.* **42**, 293–304 (2024).
1028 69. Germain, P.-L., Lun, A., Garcia Meixide, C., Macnair, W. & Robinson, M. D. Doublet
1029 identification in single-cell sequencing data using *scDblFinder*. *F1000Res.* **10**, 979 (2021).
1030 70. Aran, D. *et al.* Reference-based analysis of lung single-cell sequencing reveals a
1031 transitional profibrotic macrophage. *Nat. Immunol.* **20**, 163–172 (2019).
1032 71. Choudhary, S. & Satija, R. Comparison and evaluation of statistical error models for
1033 scRNA-seq. *Genome Biol.* **23**, 27 (2022).

1034 72. Hafemeister, C. & Satija, R. Normalization and variance stabilization of single-cell RNA-seq
1035 data using regularized negative binomial regression. *Genome Biol.* **20**, 296 (2019).
1036 73. Korotkevich, G. *et al.* Fast gene set enrichment analysis. *bioRxiv* 060012 (2016)
1037 doi:10.1101/060012.
1038 74. Jones, M. G. *et al.* Inference of single-cell phylogenies from lineage tracing data using
1039 Cassiopeia. *Genome Biol.* **21**, 1–27 (2020).
1040 75. Zorita, E., Cuscó, P. & Filion, G. J. Starcode: sequence clustering based on all-pairs
1041 search. *Bioinformatics* **31**, 1913–1919 (2015).
1042 76. *GeneOverlap: R Package for Testing and Visualizing Gene List Overlaps*. (Github).
1043 77. Therneau, T. M. Survival Analysis [R package survival version 3.8-3]. (2024).
1044 78. Edgar, R., Domrachev, M. & Lash, A. E. Gene Expression Omnibus: NCBI gene
1045 expression and hybridization array data repository. *Nucleic Acids Res.* **30**, 207–210 (2002).
1046

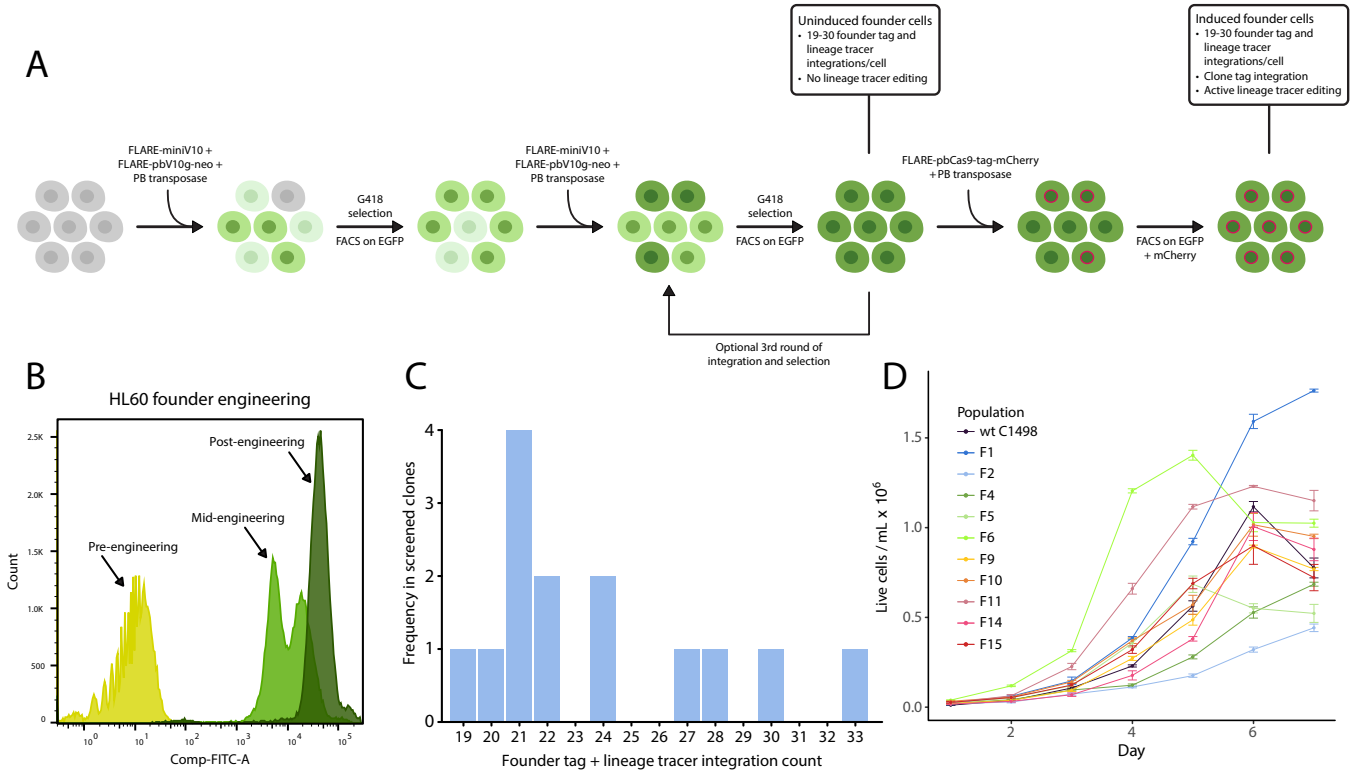

<u>Supplemental figure 1</u>: FLARE cell line engineering allows for the generation of founder populations maintaining intra-founder heterogeneity. (**A**) Schematic of engineering lineage tracing AML cells. Wildtype cells are first electroporated with FLARE-miniV10-10X-UMI + FLARE-pbV10g-neo + PB-transposase. Successfully integrated cells are selected via G418 treatment (FLARE-pbV10g-neo) and FACS for EGFP (FLARE-miniV10-10X-UMI). This process is repeated 1-2 more times, successively selecting for cells with high numbers of integrations. Once the desired number of integrations is reached, cells are considered uninduced founder cells. Prior to the start of a lineage tracing experiment, uninduced founder cells are electroporated with FLARE-pbCas9-tag-mCherry and PB-transposase and sorted on EGFP (FLARE-miniV10-10X-UMI) and mCherry (FLARE-pbCas9-tag-mCherry). Resulting cells are referred to as induced founder cells and contain all the necessary integrations for founder and clonal tracking. (**B**) FACS plots showing the increase in EGFP expression in HL60 cells through 2 rounds of electroporation with FLARE-miniV10-10X-UMI + FLARE-pbV10g-neo + PB transposase. Post-engineering uninduced HL60-FLARE founder cells uniformly express high levels of EGFP. (**C**) Uninduced C1498-FLARE founder populations were subcultured to determine founder tag and lineage recorder integration counts. Founders contained between 19 and 33 integrations. (**D**) Subcultured founder populations display a range of growth rates and carrying capacities, indicating sustained heterogeneity following the engineering process.

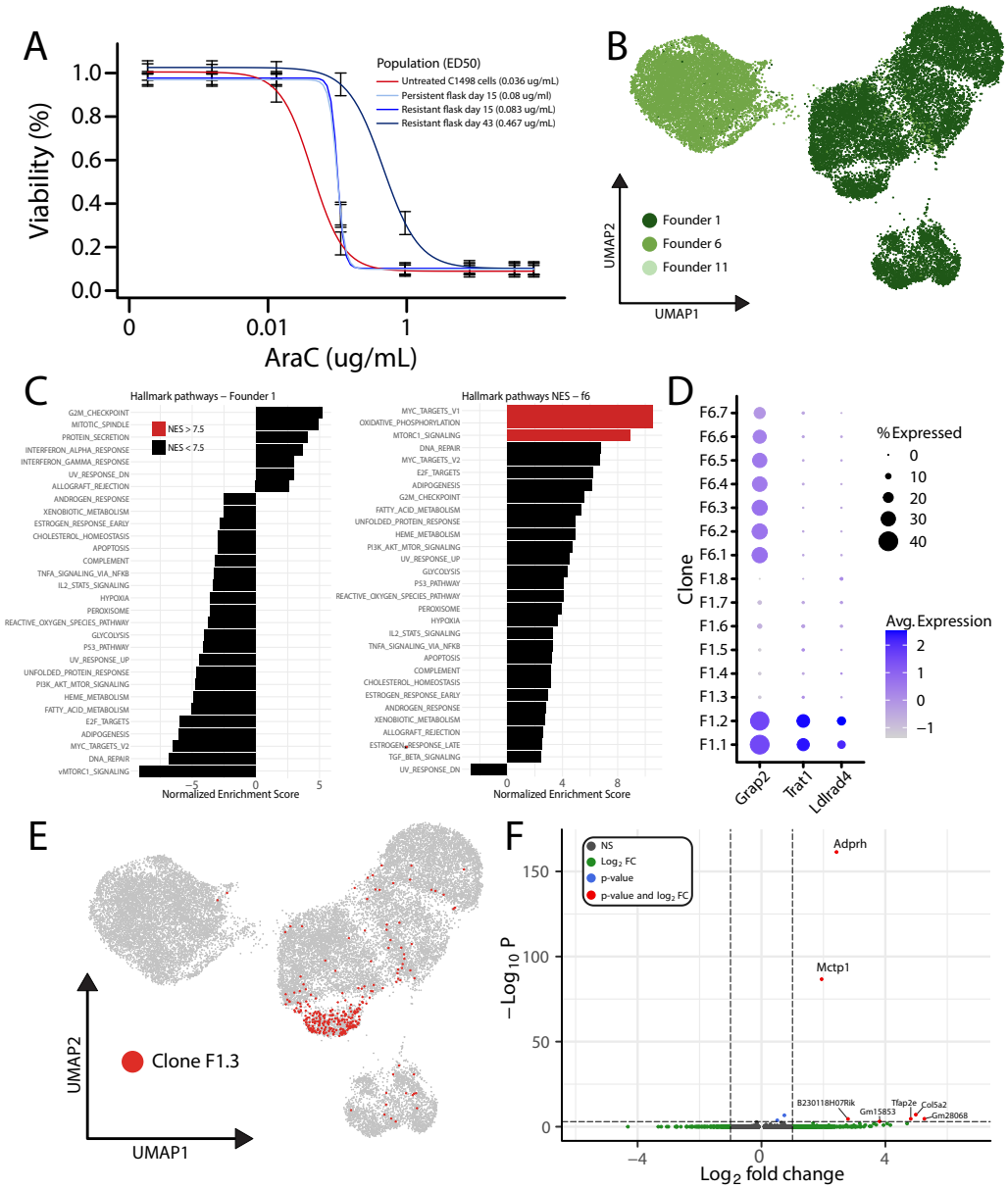

<u>Supplemental figure 2</u>: AraC treatment of C1498-FLARE cells in vitro leads to the generation of AraC-insensitive populations. FLARE recorder analysis reveals founder and clone-level transcriptomic differences. (**A**) AraC dose-response curves for C1498-FLARE cells through in vitro treatment. Cells in the resistant flask displayed an increase in ED50 values throughout treatment, indicating the emergence of an AraC-resistant population. Cells in the persistent flask also displayed an increase in ED50 values on day 15 of AraC treatment, but did not recover enough for another dose-response curve on day 43, suggesting higher AraC sensitivity compared to the resistant flask. (**B**) Captured C1498-FLARE cells colored by founder population. (**C**) GSEA analysis on founder 1 and founder 6 control cells to identify basal founder-specific differences. Analysis was conducted using the fGSEA R package and Hallmark gene sets from the mSigDB. (**D**) Dot plot showing expression of Grap2, Trat1, and Ldlrad4 in C1498-FLARE clone populations. (**E**) UMAP of C1498-FLARE cells with clone F1.3 cells highlighted in red. (**F**) Differential gene expression analysis on clone F1.3 cells compared to all founder 1 control cells uncovers clone-specific increased expression of Adprh and Mctp1.

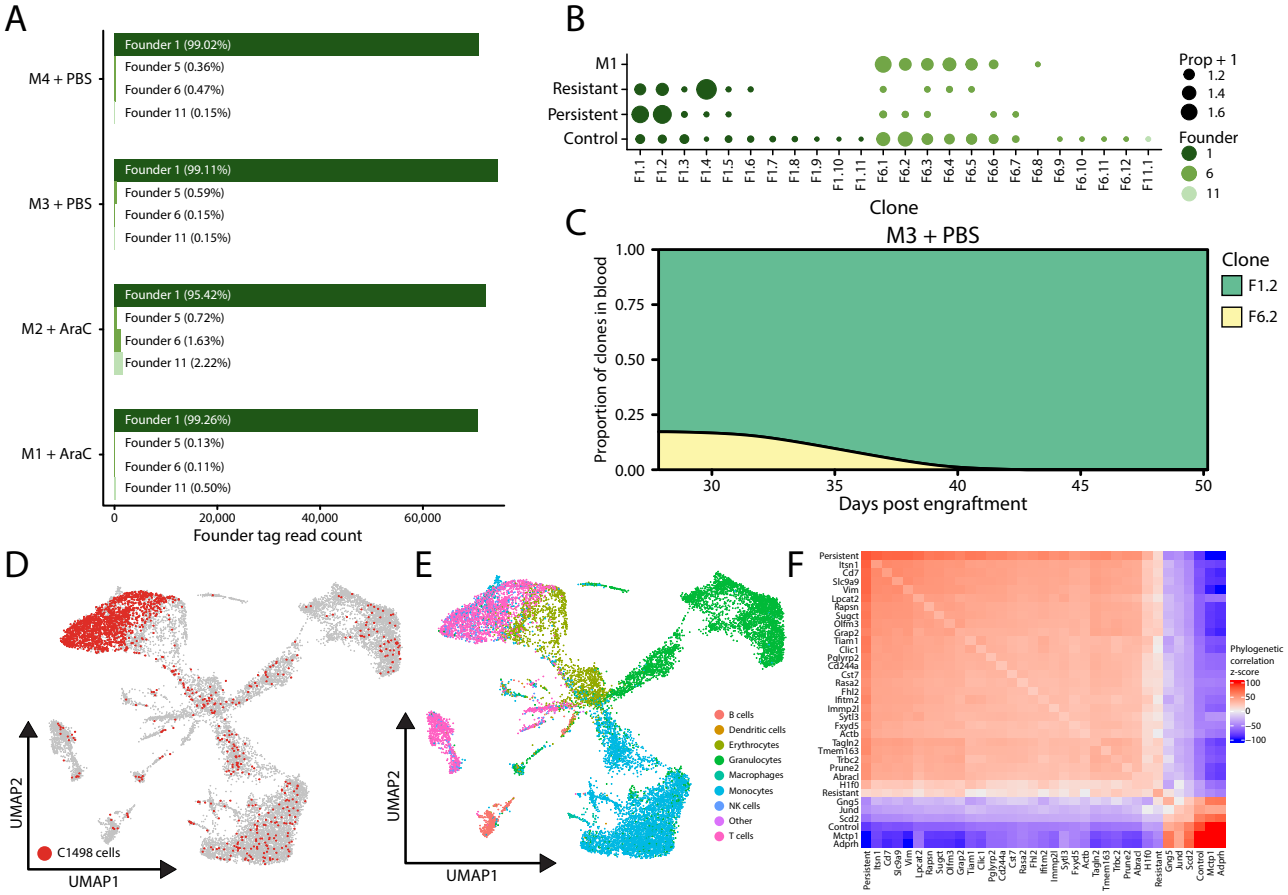

<u>Supplemental figure 3</u>: AraC treatment of C1498-FLARE cells in vivo leads to outgrowth of founder 6 cells. (**A**) Founder tag sequencing of blood draws taken 28 days after mice were injected IV with C1498-FLARE cells. (**B**) Clone populations for each sample, including in vivo sequencing from M1, first ordered by founder then by clone size. (**C**) Bulk sequencing of clone tags detected in blood draws from mouse M3. Clone tag reads were used to determine the clonal proportions of leukemic burden in the blood from day 30 to euthanasia on day 50. Founder proportions differ from figure 2E due to subsetting for clone tags detected in single cell data. (**D**) Captured single cells from endpoint blood and bone marrow collected from mouse M1. (**E**) Captured single cells from endpoint blood and bone marrow collected from mouse M1. Predicted C1498-FLARE cells were defined as having sufficient founder and clone tag reads to assign lineage identities, highlighted in red. (**F**) Cross-correlation heatmap of the top 35 auto-correlated genes over the Founder 1 tree.

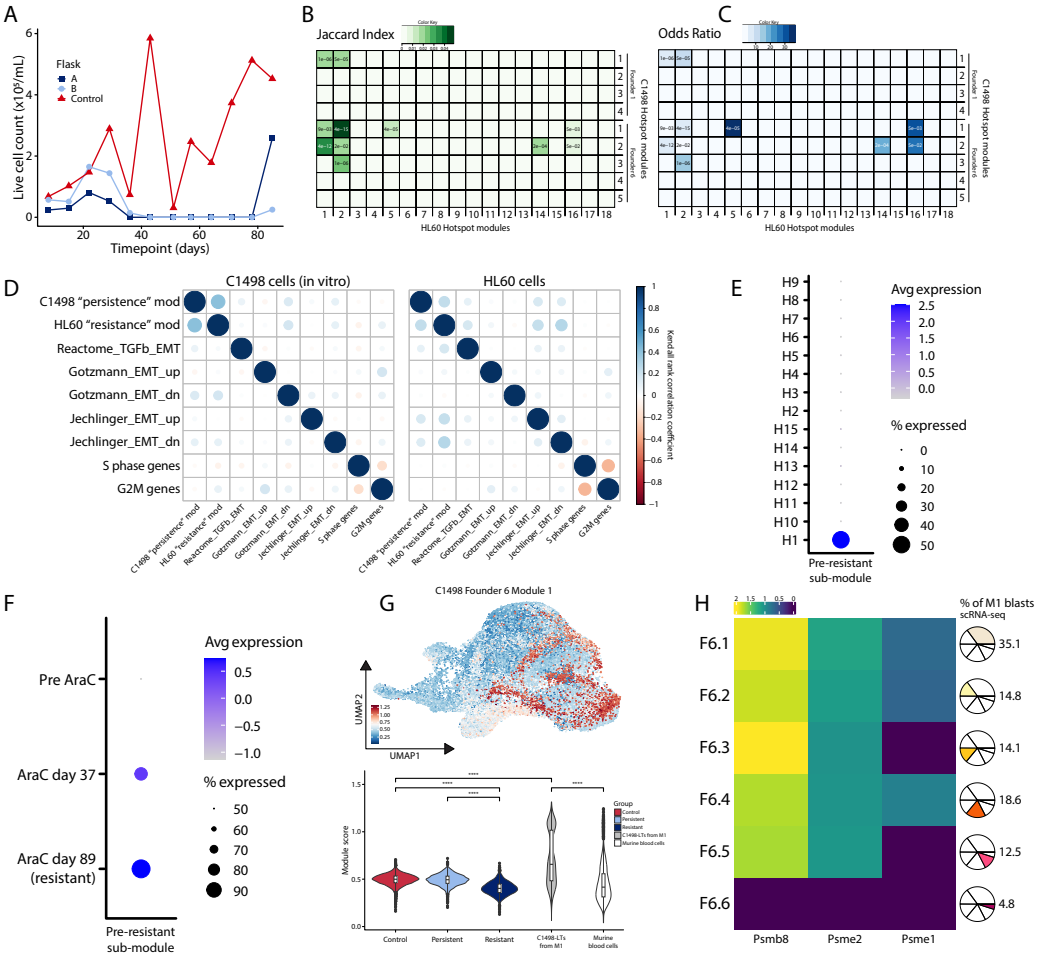

<u>Supplemental figure 4</u>: AraC treatment of HL60-FLARE cells in vitro leads to the generation of chemoresistance. Resistance-associated heritable Hotspot modules in C1498-FLARE and HL60-FLARE cells suggest the existence of drug response pathways common to murine and human AML cells. (**A**) Live cell counts for HL60-FLARE cells undergoing in vitro AraC treatment. Each flask was counted in duplicates at each timepoint, and counts were averaged. Control flask counts vary due to culture splitting in the days prior to counting. Treated flasks A and B did not have enough cells to be detected between day 40 and 80 and were not split during that time frame. (**B**) Jaccard Index similarity comparing C1498-FLARE and HL60-FLARE Hotspot modules. Square color is the Jaccard Index; values indicate BH-corrected P-values. (**C**) The odds ratio of gene overlaps comparing C1498-FLARE and HL60-FLARE Hotspot modules. Square color determined by odds ratio; values indicate BH-corrected P-values. (**D**) Expression scores for C1498 "persistence" Founder 1 module 1, HL60 "resistance" module 2, various EMT gene sets, and cell cycle gene sets are minimally correlated as measured by Kendall ranked correlation coefficient in C1498-FLARE and HL60-FLARE cells in vitro. (**E**) Dot plot showing expression of the pre-resistant sub-module in pre-experiment HL60-FLARE cells by founder. Founder H1 shows distinct upregulation of the signature. (**F**) Dot plot showing expression of the pre-resistant sub-module in AraC-treated HL60-FLARE H1 cells pre-experiment, at midpoint, and at endpoint. Pre-resistant signature expression increases through AraC treatment. (**G**) UMAP of founder 6 module 1 expression in the in vitro C1498-FLARE cells integrated with M1 endpoint sequencing. Below is expression quantification by cell group and shows module expression enrichment in cells collected from M1. (**H**) Log2 fold change values of Psmb8, Psme1, Psme2 genes for C1498-FLARE founder 6 clones comparing in vitro to in vivo clone cells.

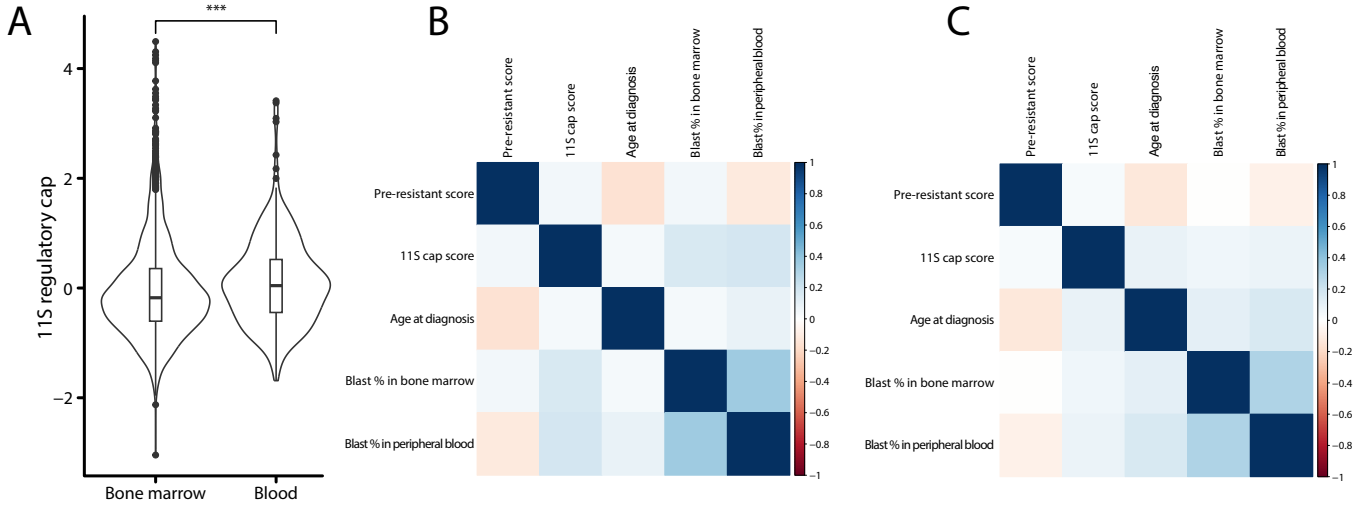

<u>Supplemental figure 5</u>: Expression of the 11S cap and pre-resistant signature are not strongly correlated with bone marrow or peripheral blood blast percentage at diagnosis. (**A**) Violin plot showing 11S regulatory cap gene set scores calculated from TARGET-AML patient samples taken at diagnosis. Mean expression in blood is significantly higher than in bone marrow. (**B**) TARGET-AML expression scores for 11S regulatory cap and pre-resistant signature in the bone marrow at diagnosis, age at diagnosis, and percentage of leukemic blasts in bone marrow and peripheral blood are minimally correlated as measured by Kendall ranked correlation coefficient. (**C**) TARGET-AML expression scores for 11S regulatory cap and pre-resistant signature in the peripheral blood at diagnosis, age at diagnosis, and percentage of leukemic blasts in bone marrow and peripheral blood are minimally correlated as measured by Kendall ranked correlation coefficient.